5-2019

Uumanned Aerial Vehicle Data Analysis For High-throughput Plant Phenotyping

Jiating Li
University of Nebraska-Lincoln, jiatingli@huskers.unl.edu

UNMANNED AERIAL VEHICLE DATA ANALYSIS FOR HIGH-THROUGHPUT PLANT PHENOTYPING

by

Jiating Li

A THESIS

Presented to the Faculty of

The Graduate College at the University of Nebraska

In Partial Fulfillment of Requirements

For the Degree of Master of Science

Major: Agricultural and Biological Systems Engineering

Under the Supervision of Professor Yeyin Shi

Lincoln, Nebraska

May, 2019

UNMANNED AERIAL VEHICLE DATA ANALYSIS FOR HIGH-THROUGHPUT PLANT PHENOTYPING

Jiating Li, M.S.

University of Nebraska, 2019

Advisor: Yeyin Shi

The continuing population is placing unprecedented demands on worldwide crop yield production and quality. Improving genomic selection for breeding process is one essential aspect for solving this dilemma. Benefitted from the advances in high-throughput genotyping, researchers already gained better understanding of genetic traits. However, given the comparatively lower efficiency in current phenotyping technique, the significance of phenotypic traits has still not fully exploited in genomic selection. Therefore, improving HTPP efficiency has become an urgent task for researchers. As one of the platforms utilized for collecting HTPP data, unmanned aerial vehicle (UAV) allows high quality data to be collected within short time and by less labor. There are currently many options for customized UAV system on market; however, data analysis efficiency is still one limitation for the fully implementation of HTPP. To this end, the focus of this program was data analysis of UAV acquired data. The specific objectives were two-fold, one was to investigate statistical correlations between UAV derived phenotypic traits and manually measured sorghum biomass, nitrogen and chlorophyll content. Another was to conduct variable selection on the phenotypic parameters calculated from UAV derived vegetation index (VI) and plant height maps, aiming to find

out the principal parameters that contribute most in explaining winter wheat grain yield. Corresponding, two studies were carried out. Good correlations between UAV-derived VI/plant height and sorghum biomass/nitrogen/chlorophyll in the first study suggested that UAV-based HTPP has great potential in facilitating genetic improvement. For the second study, variable selection results from the single-year data showed that plant height related parameters, especially from later season, contributed more in explaining grain yield.

CONTENTS

List of Multimedia Objects

CHAPTER 1 INTRODUCTION

Doubling crop production by 2050 is urgent in order to meet the increasing demands from rising human population as well as the increase in biofuel consumptions. However, study showed that current increasing rate of crop yield has not met the required rate per year (2.4%) (Araus & Cairns, 2014; Ray, Mueller, West, & Foley, 2013). It still remains as a major task for breeders to enhance crop production efficiency. Genomic selection is one of the solutions that researchers have been working on, which requires breeders to identify the best genotype with highest production rate and good resistance under given environmental conditions. Since phenotypic traits represent the interaction between genetic traits and environmental stress, it is reasonable to involve phenotypic data in genomic selection and to investigate phenotypic traits' predictive or analytic power for manually measured agronomic or physiological traits, such as biomass and grain yield. Recently, most of the phenotypic traits are derived from a procedure called high-throughput plant phenotyping (HTPP).

HTPP has increasingly been considered as a key component in crop breeding, which adopted non-destructive and non-invasive sensors to screen large amounts of crop lines with less time and efforts. The phenotypic traits derived from HTPP data are good quantitative measurements of the genotypic responses to environments (Araus, Kefauver, Zaman-Allah, Olsen, & Cairns, 2018). Nowadays, multiple remote sensing based platforms have been designed for HTPP data collections, such as ground-based platforms (Andrade-Sanchez et al., 2014; Ge, Bai, Stoerger, & Schnable, 2016; White et al., 2012) and aerial-based platforms (Chapman et al., 2014; Eitel, Long, Gessler, & Hunt, 2008;

Geipel, Link, Wirwahn, & Claupein, 2016; Kefauver et al., 2017a). Sensors attached to these platforms include, but not limited to, spectrometer, thermal sensor, and digital imager. These sensors can provide various phenotypic traits (e.g. canopy spectra, temperature, and plant height), which could help to explain genetic traits and have the potential to facilitate crop breeding process. Compare to ground-based platform, aerial-based platform, especially recently advanced unmanned aircraft vehicle (UAV), has the advantages of screening large-scale field within short time and less labor, acquiring high-quality imagery, as well as owning higher maneuverability to work on different locations (Sankaran et al., 2015; Yang et al., 2017).

Unmanned aircraft vehicle (UAV), defined as the vehicle that can fly without pilot onboard, normally includes fix-wing and multi-rotor types for agricultural applications. It usually integrates with different sensors, such as digital RGB camera, multispectral camera, infrared thermal camera, and hyperspectral camera (Hunt & Daughtry, 2018; Sankaran et al., 2015). By deploying these different types of sensors, as well as flying at low altitude, it can obtain high quality data (aerial imagery) with high spatial resolution and flexible spectral or temporal resolution. Furthermore, since the size of UAV system is usually small, it is easier to operate than field-based platforms. Therefore, the UAV-based HTPP is gaining increasing research focus for breeding and other agricultural purpose.

Existing applications of UAV in breeding could be found in a wide range of crops including sorghum, wheat, barley, corn, soybean, and tomato (M. Zhang et al., 2018). Depending on research objectives and available sensors, various crop phenotypic traits

were extracted. For instance, plant height derived from UAV acquired imagery was found to highly correlate with dry biomass in barley (Bendig et al., 2014, 2015). Plant height is one of the most frequently studied trait in UAV-based studies, and it usually combined with other UAV-derived traits to estimate agronomic or physiological traits, such as cotton yield (Chu et al., 2016). In the study of Chu (2016), the combined features tend to outperform single trait on explaining cotton yield. Another commonly measured phenotypic trait is spectral index (vegetation index, VI). Duan, Chapman, Guo and Zheng (2017) deployed UAV with multispectral camera to derive normalized difference vegetation index (NDVI). The derived NDVI had strong correlation with hand-held sensor measurement, and was also useful in estimating final wheat yield (T. Duan, Chapman, Guo, & Zheng, 2017a). Researchers also interested in investigating the usage of multi-temporal UAV data. As the study in bread wheat illustrated (Hassan, Yang, Rasheed, Jin, et al., 2018), the senescence rate could be derived using multi-temporal spectral index from UAV imagery, such as green normalized difference vegetation index and normalized difference red-edge index. Results from this study and other related studies revealed great potential of applying multi-temporal UAV imagery on monitoring crop seasonal growth.

Even though UAV technique has already been widely applied in agricultural field and allowed easier access to HTPP, there are still remaining limitations which hold back the fully implementation of this technique. One of the problem is associated with handling the large size of UAV data, either in terms of establishing well-performed estimation

models or in terms of selecting superior variables for explaining targeted agronomic traits.

Therefore, in this study, two studies were carried out with the aim of searching solutions for the aforementioned problem. One was to build statistical models that can connect UAV phenotypic traits with manually measured genetic traits (sorghum biomass, chlorophyll and nitrogen). Another was to apply variable selection on UAV-derived phenotypic traits, in the aim of finding primary variables that contribute most in winter wheat grain yield estimation. Phenotypic traits in both tasks were derived from imagery acquired by a multi-rotor UAV, carrying a RGB camera and a five-band multispectral camera. Two specific objectives were as follows:

1. To investigate the potential of using UAV-derived multispectral and morphological traits for sorghum biomass, nitrogen and chlorophyll content estimates.
2. To conduct variable selection on UAV-derived phenotypic traits, to find out the principal parameters that contribute most in explaining wheat final grain yield.

CHAPTER 2 ELUCIDATING SORGHUM BIOMASS, NITROGEN AND CHLOROPHYLL CONTENTS WITH SPECTRAL AND MORPHOLOGICAL TRAITS DERIVED FROM UNMANNED AIRCRAFT SYSTEM

Jiating Li[1], Yeyin Shi[1*], Arun-Narenthiran Veeranampalayam-Sivakumar[1], Daniel P. Schachtman[2]

[1]Department of Biological Systems Engineering, University of Nebraska-Lincoln, Lincoln, NE, USA, [2]Department of Agronomy and Horticulture, University of Nebraska-Lincoln, Lincoln, NE, USA

* Correspondence:

Name: Yeyin Shi

Email: yshi18@unl.edu

Keywords: UAV, phenotyping, multispectral, nitrogen stress, biomass, chlorophyll, plant height, canopy cover

ABSTRACT

Unmanned aircraft systems (UAS) provide an efficient way to phenotype crop morphology with spectral traits such as plant height, canopy cover and various vegetation indices (VIs) providing information to elucidate genotypic responses to the environment. In this study, we investigated the potential use of UAS-derived traits to elucidate biomass, nitrogen and chlorophyll content in sorghum under nitrogen stress treatments. A nitrogen stress trial located in Nebraska, USA, contained 24 different sorghum lines, 2 nitrogen treatments and 8 replications, for a total of 384 plots. Morphological and spectral traits including plant height, canopy cover and various VIs were derived from UAS flights with a true-color RGB camera and a 5-band multispectral camera at early, mid and late growth stages across the sorghum growing season in 2017. Simple and

This chapter was published on *Frontiers in Plant Science*: doi: 10.3389/fpls.2018.01406

multiple regression models were investigated for sorghum biomass, nitrogen and chlorophyll content estimations using the derived morphological and spectral traits along with manual ground truthed measurements. Results showed that, the UAS-derived plant height was strongly correlated with manually measured plant height (r = 0.85); and the UAS-derived biomass using plant height, canopy cover and VIs had strong exponential correlations with the sampled biomass of fresh stalks and leaves (maximum r = 0.85) and the biomass of dry stalks and leaves (maximum r = 0.88). The UAS-derived VIs were moderately correlated with the laboratory measured leaf nitrogen content (r = 0.52) and the measured leaf chlorophyll content (r = 0.69) in each plot. The methods developed in this study will facilitate genetic improvement and agronomic studies that require assessment of stress responses in large-scale field trials.

2.1 INTRODUCTION

Following rice, wheat, corn, and barley, sorghum is the fifth most important cereal crop worldwide (Ramatoulaye et al., 2016). It is widely used in human consumption, animal feed, and biofuel production (Stanton et al., 2017). As reported, in 2016, the sorghum production in the U.S. was about 12.2 million tonnes which is approximately 20% of the world sorghum production (63.93 million tonnes) (FAOSTAT, 2017). Serving as the biomass crop for biofuel production, sorghum has the advantages of an annual growth cycle, high caloric value, and low management cost (Fernandes et al., 2018). An efficient and timely method for the prediction of sorghum biomass will help to speed the development of higher biomass varieties. The benefits of sorghum as a biomass crop

This chapter was published on *Frontiers in Plant Science*: doi: 10.3389/fpls.2018.01406

could be further enhanced if genotypes with high tolerance to stresses such as reduced nitrogen or water deficit can be more easily identified, which will be facilitated by integrating sorghum genotyping and phenotyping technologies.

In the past decade, gene sequencing technology has advanced, allowing the crop genomic information to be collected much easier and more cheaply (Furbank & Tester, 2011). However, genomic selection is still hampered by the speed and ease of obtaining large amounts of phenotypic information. Traditionally, in-field phenotyping has been conducted manually, which consumes a great deal of labor and time. High-throughput phenotyping technology developed in recent years opens opportunities to automate and speed up breeding pipelines. Depending on the traits of interest and growth stages, high-throughput phenotyping can be conducted either in the lab or in the field. For the field-based phenotyping, the ground-based systems and the aerial-based systems usually work as complementary platforms to achieve the final goal of rapid and accurate trait collection. Ground-based systems such as the gantry systems (Virlet et al., 2017), cable-suspended systems (Kirchgessner et al., 2017) and mobile cart or robotic systems (Svensgaard et al., 2014) conduct proximal sensing over or under the plant canopy with little limitation on sensor weight or size. The aerial high-throughput phenotyping usually implemented with unmanned aircraft systems (UAS) operated at low altitudes which have limited sensor payloads or weight and can only detect traits remotely over the canopy. However, they are capable of covering a larger area in a shorter period of time which minimizes the measurement error caused by changes in environmental factors, and are independent of the soil condition which may hamper movement of ground based

This chapter was published on *Frontiers in Plant Science*: doi: 10.3389/fpls.2018.01406

systems. Typical types of UAS are fixed-wing, rotary-wing, and hybrid systems. A rotary-wing platform was selected in this study to conduct slow speed, low altitude and more stable phenotypic data collection for sorghum.

UAS technology has been widely used to study various traits in different crops including sorghum. Morphological traits are often measured from natural color images, i.e. RGB images, or estimated from spectral images. Sorghum and corn plant height is a trait that has been investigated in several studies using the structure from motion technique and RGB images (Hu et al., 2018; Malambo et al., 2018; Shi et al., 2016; Pugh et al., 2018; Watanabe et al., 2017)(Shi et al., 2016). Sorghum ground cover (Tao Duan et al., 2017; Potgieter et al., 2017; Shafian et al., 2018) and leaf area index (Potgieter et al., 2017; Shafian et al., 2018) were directly calculated from the RGB images or estimated using spectral information from multispectral camera. Visible morphological traits are easier to measure than physiological traits, such as chlorophyll content, nitrogen concentration, and water content. The physiological traits are often hard to be assessed by the human eye but can be detected in the infrared spectra and the variations in those important traits become more obvious if they are depicted using vegetation indices (VIs). For example, normalized difference red edge (NDRE) was used to differentiate stay-green and senescent lines in sorghum breeding (Potgieter et al., 2017). Sorghum grain yield was well correlated with the normalized difference vegetation index (NDVI) derived from a modified three-band camera (green, red, and NIR) (Stanton et al., 2017) and a multispectral camera (Shafian et al., 2018). Sorghum panicle volume was estimated from

This chapter was published on *Frontiers in Plant Science*: doi: 10.3389/fpls.2018.01406

RGB orthomosaic, DSM and point cloud (Chang, Jung, Yeom, Maeda, & Landivar, 2017).

Biomass and nitrogen status of sorghum is particularly important for the development of new higher yielding nitrogen use efficiency energy sorghum varieties for lignocellulose production. While grain sorghum is easy to harvest, energy sorghum is not because of its very large size. The main interest of growing energy sorghum is in the biomass which may be used to produce cellulosic ethanol. The crop is over 3.5 to 4.5 m high and specialized equipment which is not usually readily available is required for harvest. Therefore, the use of UAS to estimate biomass and nitrogen status of sorghum provides a highly efficiency way for breeders to improve the crop. Most of the UAS related studies on sorghum were focused on plant height, ground cover, leaf area index and grain yield estimation so far. The only study we found for sorghum biomass estimation was using a UAS based hyperspectral and RGB system and machine learning modeling (Zhang et al., 2017). The results were promising which inspired us to move forward to investigate alternative low-cost method based on multispectral and RGB cameras for sorghum biomass, nitrogen and chlorophyll content estimation. As for sorghum nitrogen and chlorophyll estimation, most of the previous studies focused on qualitative differentiation between treatments such as high and low nitrogen treatment or stay-green and senescent lines; while no study was found that investigated the quantitative relationship between sorghum nitrogen or chlorophyll content and UAS-derived traits.

This chapter was published on *Frontiers in Plant Science*: doi: 10.3389/fpls.2018.01406

The objective of this study was to investigate the potential of using UAS-derived multispectral and morphological traits for sorghum biomass, nitrogen and chlorophyll content estimates. Three specific objectives were:

(1) Obtain sorghum spectral and morphological traits from UAS based remote sensing, including various vegetation indices, plant height and canopy cover;

(2) Establish predictive models for sorghum biomass, nitrogen and chlorophyll contents using the obtained morphological and spectral traits; and

(3) Evaluate how predictions compared with ground truth measurements.

2.2 MATERIALS and METHODS

A flowchart has been provided in Figure 2.1, summarizing the main steps of this study: image data collection, image pre-processing, morphological and spectral trait extraction, and statistical analysis.

This chapter was published on *Frontiers in Plant Science*: doi: 10.3389/fpls.2018.01406

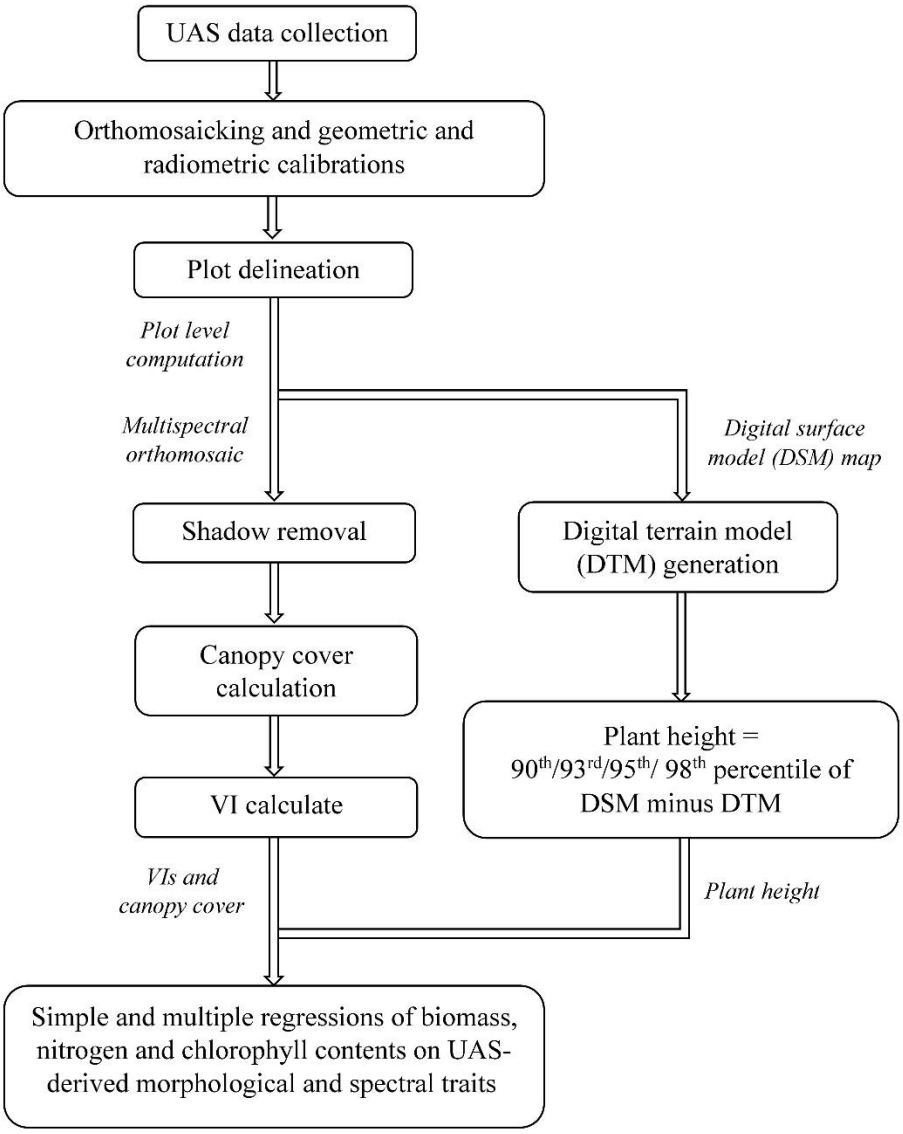

Figure 2.1. Flowchart of main processing steps in this study.

2.2.1 Field Experimental Design

Field location and plot design - The field experiment was conducted over a 1.38 ha sorghum nitrogen stress trial located in Central City, Nebraska, US (41°12'3.0'' N, 97°56'40.56'' W), in the growing season of 2017. The field was planted on May 26, 2017 with 24 sorghum lines (see Supplemental data table 1) in two nitrogen treatments (for the

low nitrogen treatment no nitrogen was applied and for the high treatment 85 pounds of nitrogen per acre were added) and eight replications in a randomized complete block design (Figure 2.2). Each plot was 3 m by 3 m containing four rows with 0.10 m within-row spacing and 0.76 m row spacing delineated by a rectangular in Figure 2. This field trail was located on a commercial farm with center pivot irrigation. Nine inches of irrigation was added contain 0.9 ppm nitrate.

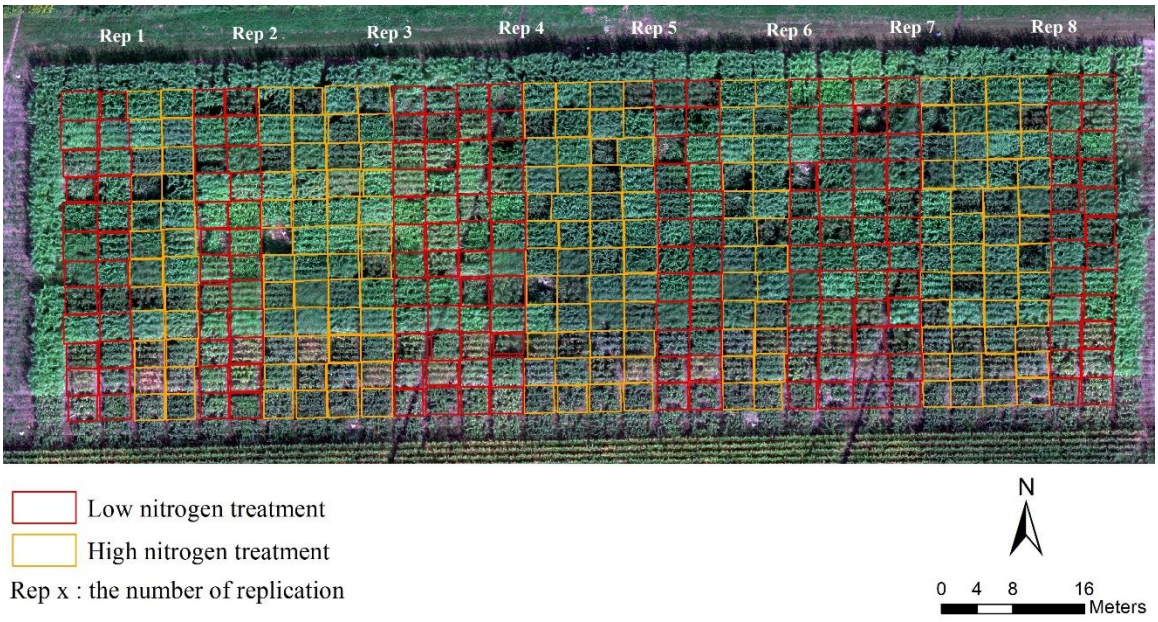

Figure 2.2. True-color orthomosaic showing field design. Images collected on September 11, 2017.

Collection of hyperspectral radiometer data - The most recently fully expanded leaf was taken from two random plants within a plot. The ASD FieldSpec 4 Standard Res (Analytical Spectral Devices, Colorado) was then used to measure hyperspectral reflectance readings in the 350 to 2500 nm wavelength range of the leaf. The methods used here for the ASD readings are described in Yendrek et al. (2017). Both ends of the

leaf were removed leaving roughly six to eight inches of the mid-section of the leaf. The leaf tissue on both sides of the midrib were removed from the midrib. One side was put into a paper envelope and dried at 50°C for nitrogen analysis and the other was placed into an aluminum foil packet which was then put on dry ice and subsequently stored at -80°C.

Laboratory analysis of leaf tissue - Frozen leaf issue was removed from -80°C and placed on dry ice. In a darkened room leaf discs (6 mm diameter) were punched from frozen leaves in the weigh boat, on dry ice until there was approximately 90 mg of leaf tissue which was about 18 to 27 discs. Prior to extraction 2.5 mL of 100% methanol was added to 15mL tubes. Three replicates containing 30mg or six to nine discs were taken and submerged in the methanol. The tubes were then placed in a rack in the dark and placed on a rotary shaker at 250 RPM for 24 hours. After 24 hours 200 mL of each sample was used to fill a 96 well black sided plate (Corning™ Costar) with a clear flat bottom, with one of the wells being filled with 200 µL of 100% methanol to be used as the blank. The top of the plate is secured with sealing film to prevent methanol evaporation. The plate was then read three times at 666 nm for chlorophyll A, 653 nm for chlorophyll B, 470 nm for carotenoids using a BioTek Synergy H1 Hybrid Reader. The chlorophyll/methanol equation (Lichtenthaler & Wellburn, 1983)(Lichtenthaler & Wellburn, 1983) was then used in to calculate chlorophyll A, chlorophyll B, and carotenoids of the extracts. The average of the three replicates was calculated for each sample. For nitrogen analysis the leaves were roughly chopped with a stainless-steel scissors in the envelopes and then sent to Ward Labs (Kearney, NE) for analysis of total nitrogen.

This chapter was published on *Frontiers in Plant Science*: doi: 10.3389/fpls.2018.01406

Field ground truth measurements - Plant height was measured on September 7, 2017 and October 9, 2017 from all eight replicates for each treatment. Plant heights were measured as the average height of plants in one of the center rows of the 4-row plot. It was measured on plants in the middle of the 3-meter row with a telescoping measuring stick which allows you to look up to align the top of the stick with top of the plants then record the height at eye level. Total above ground biomass was harvested on October 9, 2017 at which time fresh and dry above ground biomass (leaf and stem) were sampled in 363 plots. Eight replicates from each treatment were measured. A 0.91 m section of row in the middle of the plots was identified and plants were cut down at the bottom of the stem at soil level. Stalks with leaves and panicles were weighed and recorded separately on scales in the field but only the weight of stalks with leaves were used as the fresh biomass in this study. Subsamples of three stalks with leaves were reweighed to get the fresh weight and then bagged, oven dried and used to calculate the dry to fresh weight ratios which was then used to calculate the dry weights of the plots.

2.2.2 UAS, Sensors and Flights

The system used for image capture was a Matrice 600 Pro multi-rotor UAS platform (DJI, Shenzhen, China), equipped with a Zenmuse X3 RGB camera (DJI, Shenzhen, China) and a multispectral camera RedEdge (MicaSense, Seattle, UAS). The RGB camera has 4000 by 2250 effective pixels. The multispectral camera system has five spectral bands blue, green, red, red edge and near infrared (Table 2.1), each with 1280 by 960 effective pixels, and a downwelling light sensor system installed horizontally on top of the UAS used to measure the environmental irradiance and post-calibrate reflectance

readings. As another source of radiometric calibration data, a standard calibration panel came with the multispectral camera was imaged on the ground before or after each flight.

Three flights were conducted on July 17, August 19, and September 11 in 2017. Flights were auto-piloted using DJI GO and DJI GS Pro applications with 92% forward and side overlap between images at 30 m above ground level. The resulting ground sampling distance (GSD) was 1.3 cm/pixel for RGB image and 2.0 cm/pixel for the multispectral image. The flight altitude and image acquisition parameters were tested and determined to optimize the flight duration and the quality of mosaicked maps. Eleven ground control points (GCPs) were distributed along the edges and inside the field each time before the flight for geometric calibration in image processing. Their geo-coordinates were accurately measured by a survey-grade RTK-GPS with less than 3 cm level accuracy.

Table 2.1. Center wavelength and full width at half maximum (FWHM) bandwidth of each spectral band of the RedEdge multispectral camera.

Spectral Band	Center Wavelength (nm)	Bandwidth FWHM (nm)
Blue	475	20
Green	560	20
Red	668	10
Red Edge	717	10
Near Infrared	840	40

2.2.3 Image Pre-processing

Two main tasks were completed in the pre-processing stage: the orthomosaic map and digital surface model (DSM) generation with proper geometric and radiometric calibrations; and the plot delineation to prepare for later processing.

This chapter was published on *Frontiers in Plant Science*: doi: 10.3389/fpls.2018.01406

RGB images were mosaicked by Pix4Dmapper software (Pix4D, Lausanne, Switzerland). Basically, there were three steps in Pix4Dmapper: Initial Processing; Point Cloud and Mesh; DSM, Orthomosaic and Index. In the initial processing, RGB raw images were imported into to extract and match key-points among neighboring images to form a rough mosaic. Geo-coordinates of the centers of GCPs were imported for geometric calibration and improving the initial mosaicking to form 3D point cloud and mesh. The final outputs were the 2D orthomosaic and DSM.

Multispectral images were mosaicked by Atlas Cloud service (MicaSense, Seattle, USA). Radiometric calibration was automatically addressed during this process using the irradiance measured in the field from the standard calibration panel and downwelling light sensor. The five-layer, 16-bit GeoTIFF output from Atlas was converted to five-layer reflectance GeoTIFF following the sensor instruction with a pixel value of 32768 equal to 100% reflectance. The multi-layer reflectance orthomosaic generated from the multispectral images were used later to estimate canopy cover and calculated various vegetation indices.

In order to conduct plot-based analysis, each plot boundary was delineated in the multispectral orthomosaic and DSM maps with unique plot ID as shapefiles in ArcGIS (Figure 2.2). The shapefiles, DSMs and multispectral orthomosaics were exported to R software for further data analysis.

Shaded area would affect the reflectance recorded by camera, which was more pronounced when the plant was bigger. For the data set collected on the last date when sorghum plants were at their maximum height, more shadows were cast over neighboring

shorter vegetation rows and soil. This was noticed in the multispectral images where shadowed vegetation and soil pixels had abnormally higher VI values than the sunlit vegetation pixels (Figure 2.3(b)) which was also observed in previous studies (Woebbecke et al., 1995). Those pixels with abnormal VI values were filtered out in this study and only sunlit vegetation pixels were used for VI calculation in each plot. To eliminate the shadow interference on plant VI calculation, the ExG index (Table 2.2) map, which was applied in other studies in distinguishing vegetative areas from soil or residue background (D. M. Woebbecke et al., 1995), was calculated. In this study, both the soil and shaded vegetation pixels in the ExG index map had lower values than the sunlit vegetation pixels (Figure 2.3(c)) so that they were filtered out and only the sunlit vegetation pixels were retained for VI calculation. A threshold of 0.046 was determined by trial and error and used to segment the vegetation pixels from the soil pixels in the ExG map (Figure 2.3(d)). The segmented vegetation pixels formed a mask which was applied in the further processing for ground cover estimate and VI calculations.

Table 2.2. Formulas of vegetation indices used in this study.

VIs	Formula	Feature / application
ExG	$2 \times \rho_{Green} - \rho_{Red} - \rho_{Blue}$	Distinguishes vegetation from soil background
NDVI	$(\rho_{NIR} - \rho_{Red})/(\rho_{NIR} + \rho_{Red})$	Correlates with green biomass, chlorophyll
RDVI	$(\rho_{NIR} - \rho_{Red})/\sqrt{(\rho_{NIR} + \rho_{Red})}$	Less sensitive to the interfering effects of soil
GNDVI	$(\rho_{NIR} - \rho_{Green})/(\rho_{NIR} + \rho_{Green})$	Correlates with *Chlorophyll-a*
CI_{Green}	$(\rho_{NIR}/\rho_{Green}) - 1$	Correlates with chlorophyll and nitrogen
$CI_{RedEdge}$	$(\rho_{NIR}/\rho_{RedEdge}) - 1$	Correlates with chlorophyll and nitrogen
NDRE	$(\rho_{NIR} - \rho_{RedEdge})/(\rho_{NIR} + \rho_{RedEdge})$	Correlates with chlorophyll or nitrogen
RGBVI	$(\rho_{Green}{}^2 - \rho_{Blue} \times \rho_{Red})/(\rho_{Green}{}^2 + \rho_{Blue} \times \rho_{Red})$	Estimates biomass

* ρ means spectral reflectance.

This chapter was published on *Frontiers in Plant Science*: doi: 10.3389/fpls.2018.01406

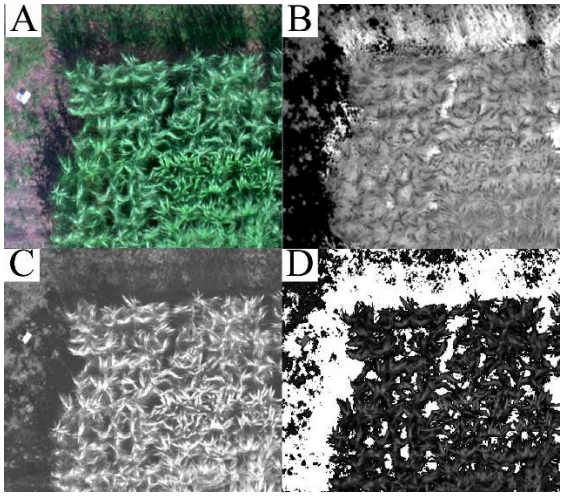

Figure 2.3. Shadow removal and vegetation segmentation from soil background using an example plot. (A) the RGB composite of the multispectral mosaic, (B) NDVI map showing the shaded area had higher NDVI values than canopy pixels, (C) excess green (ExG) image in which both the soil and shaded pixels have lower values than the sunlit vegetation pixels, and (D) mask for vegetation pixels (white pixels are soil and shaded pixels).

2.2.4 Morphological and Spectral Traits Extraction

Morphological and spectral plant traits were extracted from the pre-processed data to estimate sorghum biomass and nitrogen and chlorophyll contents, including plant height, canopy cover, and various VIs at the individual plot level.

Plant height was derived by subtracting the digital terrain model (DTM) from the digital surface model (DSM). The DSM was generated along with the orthomosaic from mosaicking the RGB images in Pix4D, and was geometrically calibrated with the GCP's coordinates surveyed by the RTK-GPS during field data collections. The DTM was generated by linearly interpolating the soil surface on east and west side of the field,

This chapter was published on *Frontiers in Plant Science*: doi: 10.3389/fpls.2018.01406

assuming little elevation changes within this 1.38 ha field. The derived plant height map had the same spatial resolution of 1.3 cm as the RGB orthomosaic. The 90^{th}, 93^{rd}, 95^{th}, and 98^{th} percentiles of all pixels falling into a plot boundary were calculated and compared with the manually sampled plant height in the same plot to find the one with highest correlation. After shadow removal, canopy cover was calculated as the ratio of the number of segmented sunlit vegetation pixels to the total number of pixels in a plot (Lee & Lee, 2011).

Calibrated reflectance in each multispectral band was extracted, and various VIs were calculated for each plot by averaging the VI values of all pixels of interest within the plot boundary. These VIs included normalized difference vegetation index (NDVI), renormalized difference vegetation index (RDVI) (Roujean & Breon, 1995), green normalized difference vegetation index (GNDVI) (Gitelson et al., 1996), green chlorophyll index (CI_{Green}) and red edge chlorophyll index ($CI_{RedEdge}$) (Schlemmera et al., 2013), normalized difference red edge index (NDRE) (Fitzgerald et al., 2006), and RGB vegetation index (RGBVI) (Bendig et al., 2015) (Table 2.2). NDVI is one of the most commonly used indices for estimating crop physiological traits such as chlorophyll. RDVI uses the same spectral bands as NDVI; however, RDVI is less sensitive to the variation of soil background. Given the saturation problem of NDVI after canopy closure, RDVI may be considered superior (Fu et al., 2013). GNDVI was found to have wider dynamic range than NDVI and is more sensitive to *chlorophyll-a* concentration (Gitelson et al., 1996). Similar to NDVI, NDRE is a good indicator of chlorophyll or nitrogen status (Fitzgerald et al., 2006); however, the replacement of red band with the red edge

This chapter was published on *Frontiers in Plant Science*: doi: 10.3389/fpls.2018.01406

band makes NDRE more sensitive to the biomass change than NDVI after canopy closure. Using bands in the visible spectra, RGBVI can be used to estimate biomass (Bendig et al., 2015).

2.2.5 Statistical Modeling for Biomass, Nitrogen and Chlorophyll Contents

Since the biomass was sampled late in the season close to the last flight date, only the UAS data collected on September 11, 2017 was used for the biomass analysis. To estimate the fresh and dry biomass using remotely sensed plant traits, simple exponential regression (SER) models were first built using univariate morphological or spectral trait. Given that the biomass is intuitively related to multiple traits such as plant height, and stalk diameter, it is also worth investigating the integration of more than one trait using multiple exponential regression (MER) models to see if the estimation of biomass can be improved. To select predictors for the MER models, a correlation matrix was first calculated to avoid including predictors that were highly correlated (Table 2.3). In this study, Pearson's correlation coefficient r was used and the strength of the correlation was determined as summarized by Asuero, Sayago, and González (2006): r ranging from 0 to 0.29 was interpreted as little if any correlation, r ranging from 0.30 to 0.49 was regarded as low correlation, and r ranging from 0.50 to 0.69 was moderate correlation, while r greater than 0.69 was high to very high correlation. In this study, paired predictors with r lower than 0.69 were selected to be included in the regression models. Based on that, the following ten combinations of predictors were investigated: plant height and canopy cover, NDVI and RGBVI, NDRE and RGBVI, RDVI and RGBVI, plant height and

This chapter was published on *Frontiers in Plant Science*: doi: 10.3389/fpls.2018.01406

NDRE, plant height and RGBVI, canopy cover and NDVI, canopy cover and NDRE, canopy cover and RDVI, plant height and canopy cover and NDRE.

Table 2.3. Correlation matrix of candidate predictors in biomass prediction. r ranging from 0 to 0.29 was interpreted as little if any correlation (highlighted in blue), r ranging from 0.30 to 0.49 was regarded as low correlation, and r ranging from 0.50 to 0.69 was moderate correlation (highlighted in yellow), and r greater than 0.69 was high to very high correlation.

	Plant height	Canopy cover	NDVI	NDRE	RDVI	RGBVI
Plant height	1					
Canopy cover	0.61	1				
NDVI	0.74	0.54	1			
NDRE	0.68	0.25	0.90	1		
RDVI	0.80	0.57	0.96	0.89	1	
RGBVI	0.54	0.75	0.64	0.26	0.59	1

363 samples from the September 11 flight were divided into training set (290 samples) and testing set (73 samples) in a ratio of 4:1. The training set was used to build regression models which were validated using 10-fold cross validation. The validation results were reported using averaged root mean square error (*RMSE*) of the 10 folds (Eq. 1) and standard deviation (*STD*) (Eq. 2) of 10 *RMSE* values derived from the 10-fold cross validation. The established regression models were further tested using the testing set, and were evaluated using the Pearson correlation coefficients (*r*) (Eq. 3) and *RMSE*.

$$RMSE = \sqrt{\frac{1}{n}\sum_{i=1}^{n}(P_i - M_i)^2} \quad (1)$$

$$STD = \sqrt{\frac{\sum_{i=1}^{n}(x_i - \bar{x})^2}{n-1}} \quad (2)$$

$$r = \frac{\sum_i^n (M_i - \bar{M})(P_i - \bar{P})}{\sqrt{\sum_i^n (M_i - \bar{M})^2}\sqrt{\sum_i^n (P_i - \bar{P})^2}} \quad (3)$$

This chapter was published on *Frontiers in Plant Science*: doi: 10.3389/fpls.2018.01406

where n is the number of samples, P_i stands for predicted value, M_i stands for manually measured value, $\bar{P}$ is the mean of predicted values, $\bar{M}$ is the mean of manually measured values. x_i is the observed values, and $\bar{x}$ is the mean value of these observations.

In order to examine the effect of nitrogen treatments, t-tests were conducted using three VIs (CI_{Green}, $CI_{RedEdge}$, and NDRE) calculated from the last flight (September 11, 2017) between high nitrogen (192 plots) and low nitrogen (192 plots) treatments.

Furthermore, to evaluate the relationship between various VIs and sorghum chlorophyll and nitrogen contents, *r* was calculated between the various VIs and the manually measured leaf chlorophyll and nitrogen contents for sampled sorghum plants from each plot. For chlorophyll, 70 plots in July, 68 plots in August, and 112 plots in September had valid samples (250 samples in total); for nitrogen, 50 plots in July, 50 plots in August, and 69 plots in September had valid samples (169 samples in total).

2. 3 RESULTS

2.3.1 Plant Height Estimation

Compared to other percentile values, a stronger linear correlation was obtained (r = 0.85) between the 90th percentile of estimated plant height from the RGB orthomosaic and the manually sampled plant height in 363 plots in September 2017 (Figure 2.4). The *RMSE* was 49.8 cm and the *r* was 0.85 between UAS derived plant height and manually measured plant height. The coefficient of variation (CV) for aerial data estimated plant height was 32.11% and for manually measured plant height was 27.92%.

This chapter was published on *Frontiers in Plant Science*: doi: 10.3389/fpls.2018.01406

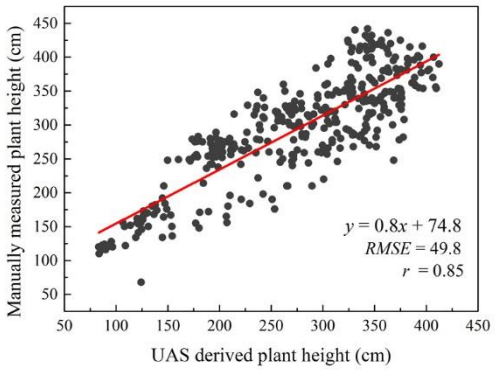

Figure 2.4. Correlation between UAS estimated plant height and manually measured plant height over 363 plots on September 11, 2017.

2.3.2 Fresh and Dry Biomass Estimation

The correlations between a single UAS-derived morphological or spectral trait and the manually sampled fresh or dry biomass tended to be exponential rather than linear in this study (Figure 2.5).

For the simple exponential model of fresh biomass (Table 2.4), plant height gave higher correlation than canopy cover (r = 0.81), whereas RDVI and NDVI provided better results than the other VIs (r = 0.83 for RDVI, and r = 0.80 for NDVI).

Slightly better correlations were obtained when multiple traits were combined into the fresh biomass regression model, with the outcome being that r was greater than 0.80 for all combinations. Interestingly, when used individually in the simple exponential models, either NDRE or RGBVI resulted in lower correlations (r = 0.66 for NDRE, r = 0.57 for RGBVI); however, the combination of them using the multiple exponential model largely improved the correlation with fresh biomass (r = 0.82). Similar results were found in

This chapter was published on *Frontiers in Plant Science*: doi: 10.3389/fpls.2018.01406

prediction of dry biomass. The morphological trait plant height (r = 0.87), spectral traits RDVI (r = 0.78) and NDVI (r = 0.78) individually exhibited better correlations with the dry biomass using simple exponential models; while the combination of them with other traits did not significantly improve the results in this case (Table 2.5).

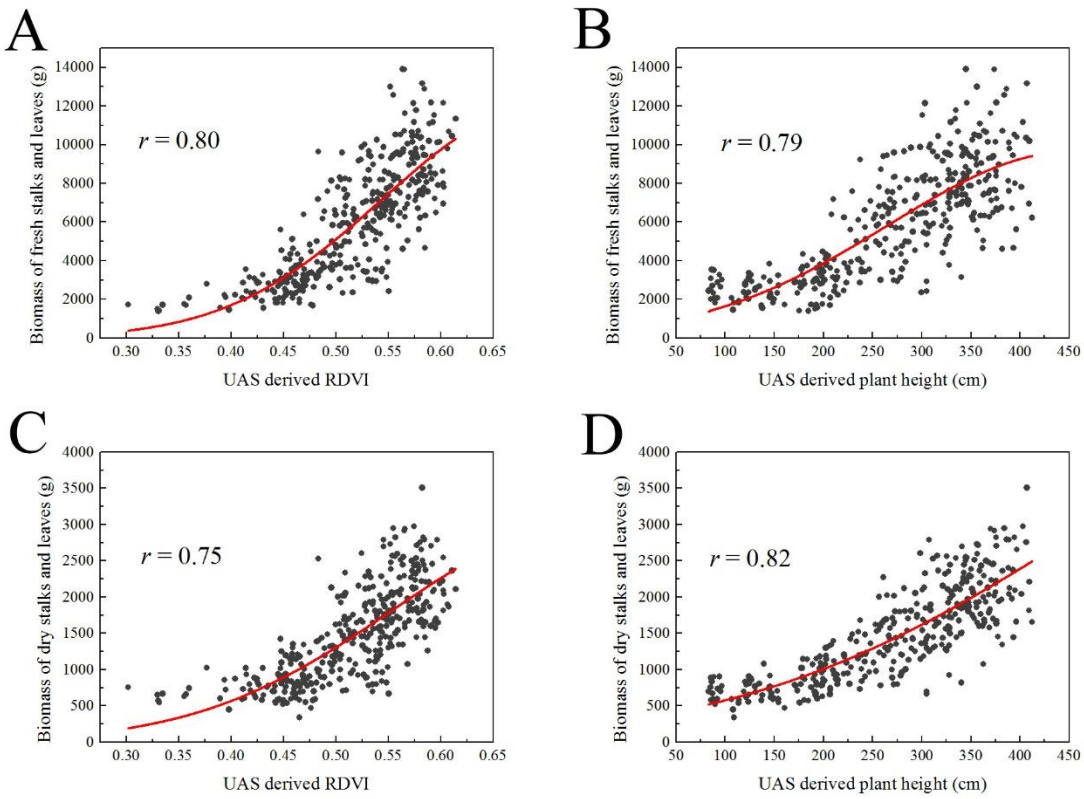

Figure 2.5. Exponential correlations between some UAS-derived traits and the manually sampled biomass of stalks and leaves (fresh or dry), over 363 plots: (A) RDVI and fresh biomass, (B) plant height and fresh biomass, (C) RDVI and dry biomass, (D) plant height and dry biomass.

This chapter was published on *Frontiers in Plant Science*: doi: 10.3389/fpls.2018.01406

Table 2.4. Fresh biomass estimation results in 10-fold cross validation as well as in the testing set, based on simple exponential regression (SER) and multiple exponential regression (MER) models.

Model	Predictors	Training set: average of 10-fold cross validation		Formula*	Testing set	
		RMSE (kg)	*STD* (kg)		*RMSE* (kg)	*r*
SER	Plant height	23.78	4.06	$Y = 21.22 \times e^{(0.005 \times PH)}$	26.25	0.81
	Canopy cover	32.30	5.16	$Y = 22.47 \times e^{(1.618 \times CC)}$	35.78	0.62
	NDVI	23.67	3.11	$Y = 0.31 \times e^{(7.03 \times NDVI)}$	25.89	0.80
	NDRE	28.19	3.40	$Y = 14.02 \times e^{(3.813 \times NDRE)}$	31.88	0.66
	RDVI	18.10	3.60	$Y = 2.04 \times e^{(6.973 \times RDVI)}$	24.26	0.83
	RGBVI	32.73	4.69	$Y = 6.41 \times e^{(3.68 \times RGBVI)}$	36.79	0.57
MER	Plant height and canopy cover	23.73	4.10	$Y = 18.70 \times e^{(0.004 \times PH + 0.246 \times CC)}$	25.98	0.81
	NDVI and RGBVI	23.69	3.11	$Y = 0.26 \times e^{(6.637 \times NDVI + 0.706 \times RGBVI)}$	25.62	0.80
	NDRE and RGBVI	23.89	3.57	$Y = 1.36 \times e^{(3.605 \times NDRE + 3.571 \times RGBVI)}$	24.92	0.82
	RDVI and RGBVI	23.25	3.54	$Y = 1.32 \times e^{(6.41 \times RDVI + 1.069 \times RGBVI)}$	23.70	0.84
	Plant height and NDRE	23.32	3.81	$Y = 16.54 \times e^{(0.004 \times PH + 1.166 \times NDRE)}$	25.54	0.81
	Plant height and RGBVI	23.31	3.92	$Y = 9.37 \times e^{(0.004 \times PH + 1.370 \times RGBVI)}$	25.14	0.83
	Canopy cover and NDVI	23.01	3.28	$Y = 0.31 \times e^{(0.584 \times CC + 6.447 \times NDVI)}$	24.81	0.82
	Canopy cover and NDRE	24.35	3.89	$Y = 5.86 \times e^{(1.336 \times CC + 3.486 \times NDRE)}$	25.76	0.80
	Canopy cover and RDVI	23.10	3.81	$Y = 1.96 \times e^{(0.434 \times CC + 6.412 \times RDVI)}$	23.81	0.83
	Plant height, canopy cover, and NDRE	22.82	3.89	$Y = 10.63 \times e^{(0.003 \times PH + 0.6 \times CC + 1.728 \times NDRE)}$	24.47	0.83

* *STD* is standard deviation of 10 *RMSE* values of the total plot weight from the 10-fold cross validation; Y is the predicted fresh biomass (kg/plot); PH is the plant height; CC is the canopy cover; NDVI is the normalized difference vegetation index, NDRE is the normalized difference red edge index, RDVI is the renormalized vegetation index, and RGBVI is the RGB vegetation index.

Table 2.5. Dry biomass estimation results in 10-fold cross validation as well as in the testing set, based on simple exponential regression (SER) and multiple exponential regression (MER) model.

Model	Predictor(s)	Training set: average of 10-fold cross validation		Formula*	Testing set	
		RMSE (kg)	*STD (kg)*		*RMSE* (kg)	*r*
SER	Plant height	4.83	0.70	$Y = 5.63 \times e^{(0.004 \times PH)}$	4.89	0.87
	Canopy cover	7.20	0.93	$Y = 6.50 \times e^{(1.42 \times CC)}$	7.89	0.59
	NDVI	5.73	0.67	$Y = 0.22 \times e^{(5.679 \times NDVI)}$	5.92	0.78
	NDRE	6.34	0.78	$Y = 4.46 \times e^{(3.272 \times NDRE)}$	6.70	0.70
	RDVI	5.58	0.69	$Y = 0.91 \times e^{(5.869 \times RDVI)}$	5.83	0.78
	RGBVI	7.51	0.74	$Y = 3.04 \times e^{(2.726 \times RGBVI)}$	8.41	0.48
MER	Plant height and canopy cover	4.82	0.70	$Y = 5.15 \times e^{(0.004 \times PH + 0.169 \times CC)}$	4.88	0.87
	NDVI and RGBVI	5.74	0.67	$Y = 0.22 \times e^{(5.607 \times NDVI + 0.130 \times RGBVI)}$	5.92	0.78
	NDRE and RGBVI	5.75	0.73	$Y = 0.86 \times e^{(3.125 \times NDRE + 2.522 \times RGBVI)}$	5.74	0.79
	RDVI and RGBVI	5.58	0.69	$Y = 0.77 \times e^{(5.664 \times RDVI + 0.392 \times RGBVI)}$	5.82	0.78
	Plant height and NDRE	4.81	0.68	$Y = 5.03 \times e^{(0.004 \times PH + 0.545 \times NDRE)}$	4.78	0.87
	Plant height and RGBVI	4.82	0.68	$Y = 4.47 \times e^{(0.004 \times PH + 0.384 \times RGBVI)}$	4.87	0.87
	Canopy cover and NDVI	5.59	0.53	$Y = 0.22 \times e^{(0.61 \times CC + 5.085 \times NDVI)}$	5.71	0.79
	Canopy and NDRE	5.52	0.56	$Y = 1.94 \times e^{(1.222 \times CC + 3.041 \times NDRE)}$	5.40	0.82
	Canopy cover and RDVI	5.49	0.69	$Y = 0.86 \times e^{(0.472 \times CC + 5.278 \times RDVI)}$	5.74	0.78
	Plant height, canopy cover, and NDRE	4.76	0.67	$Y = 3.90 \times e^{(0.003 \times PH + 0.345 \times CC + 0.87 \times NDRE)}$	4.68	0.88

* *STD* is standard deviation of 10 *RMSE* values of the total plot weight from the 10-fold cross validation; Y is the predicted dry biomass (kg/plot); PH is the plant height; CC is the canopy cover; NDVI is the normalized difference vegetation index, NDRE is the normalized difference red edge index, RDVI is the renormalized vegetation index, and RGBVI is the RGB vegetation index.

As shown in Table 2.6, significant differences were found in the remotely sensed three VIs between high and low nitrogen treatments ($p < 0.0001$). It is shown in Figure 2.6 that the nitrogen effect can be clearly distinguished with the three selected VIs - CI_{Green}, $CI_{RedEdge}$, and NDRE - derived from the late season UAS data.

Table 2.6. Student's t-test results showing significant differences of remotely sensed VIs between low (192 plots) and high (192 plots) nitrogen treatments.

VI	*t*	*p*-value
CI_{Green}	9.8025	< 2.2e-16
$CI_{RedEdge}$	9.5994	< 2.2e-16
NDRE	9.1623	< 2.2e-16

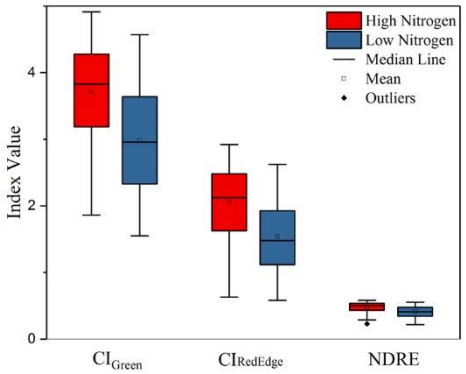

Figure 2.6. Boxplot of three VIs (CI_{Green}, $CI_{RedEdge}$, and NDRE) derived from the late season multispectral images of the low and high nitrogen treatments.

2.3.4 Chlorophyll and Nitrogen Content Estimation

Moderate to strong correlations ($r > 0.5$) were found between the chlorophyll content of leaf samples and the corresponding VIs, except NDVI, of same plots calculated from multispectral aerial data over July, August, and September in 2017 (Table 2.7). Similar

results were found for the nitrogen content (Table 2.7). These VIs included CI_{Green}, $CI_{RedEdge}$, GNDVI, and NDRE. VIs were also calculated from the leaf-level hyperspectral measurements sampled in the same plots. Similar correlations ($r > 0.4$) were found when the specific spectral bands were taken from the hyperspectral radiometer data as those calculated from the multispectral aerial data (Table 2.7). Although correlation using NDVI improved with the hyperspectral radiometer, the NDVI index had lower correlations with chlorophyll and nitrogen contents than other VIs, while NDRE remained the VI with highest correlation with nitrogen and chlorophyll in this case.

Table 2.7. Pearson correlation coefficients between the chlorophyll and nitrogen contents of leaf samples, and the corresponding VIs of same plots calculated from multispectral aerial data and leaf-level hyperspectral measurements, using data set collected over three flights in 2017.

Sensor	Traits	Chlorophyll		Nitrogen %	
		r	p-value	r	p-value
MicaSense RedEdge® multispectral camera (on UAS)	CI_{green}	0.53***	<2.2e-16	0.55***	6.65e-15
	$CI_{RedEdge}$	0.53***	<2.2e-16	0.58***	<2.2e-16
	GNDVI	0.55***	<2.2e-16	0.58***	2.588e-16
	NDVI	0.17**	0.0088	0.31***	3.736e-5
	NDRE	0.55***	<2.2e-16	0.61***	<2.2e-16
ASD FieldSpec® hyperspectral sensor with leaf clip (only the same spectral bands as RedEdge® were used)	CI_{green}	0.42***	6.733e-12	0.55***	6.899e-15
	$CI_{redEdge}$	0.50***	<2.2e-16	0.60***	<2.2e-16
	GNDVI	0.44***	3.247e-13	0.58***	<2.2e-16
	NDVI	0.27***	1.731e-5	0.42***	1.014e-8
	NDRE	0.51***	<2.2e-16	0.62***	<2.2e-16

*** Correlation is significant at the 0.001 level
** Correlation is significant at the 0.01 level

2.4 DISCUSSION

The moderate to strong correlations (*r* varied from 0.55 to 0.88) found between the UAS-derived plant morphological and spectral traits and the sorghum late-season biomass, nitrogen and chlorophyll contents in this study indicates that UAS should be useful for

phenotyping. Compared with the hyperspectral reflectance that was manually sampled at the leaf level using hyperspectral radiometer with a leaf clip, the UAS-derived VIs using the five-band multispectral camera resulted in similar correlations with nitrogen and chlorophyll contents when the same VIs were calculated from the measured hyperspectral reflectance (Table 2.7). This not only demonstrates the fidelity of the UAS-based remote spectral sensing, but also indicates the potential for scaling up the high-throughput phenotyping from ground-based leaf level to UAS-based canopy level assessment.

When a single trait was used for prediction with simple exponential regression models, estimated plant height, RDVI and NDVI indices individually had the strongest correlations with both fresh and dry sorghum biomass among the various remotely sensed traits. The high and robust correlation derived from plant height was also found in a previous study in barley (Bendig et al., 2015). Interestingly, the NDRE index showed a little lower correlation to fresh and dry biomass (r within 0.66 and 0.70) than NDVI and NDRE but significantly outperformed NDVI in chlorophyll and nitrogen content estimations (Table 2.7) which showed NDRE's known advantage over NDVI after canopy closure due to the saturation in the red spectral band at the mid to late growth stages (Mutanga & Skidmore, 2004). Late season canopy cover had moderate correlations with biomass (r within 0.59 and 0.62) but was not shown to be superior to vegetation indices in our study. The inferior correlation of RGBVI index with biomass compared with other traits was also reported in barley (Tilly et al., 2015). However, it is noteworthy that, if no near-infrared spectral data and only the RGB information was

This chapter was published on *Frontiers in Plant Science*: doi: 10.3389/fpls.2018.01406

available, the UAS-derived RGBVI index alone still provided low to moderate correlations with fresh and dry biomass (*r* within 0.48 and 0.57).

When several traits with multiple exponential regression models were used, similar correlations were achieved for fresh and dry biomass prediction as compared to the results derived from single traits in this study. The correlation using several traits was best when using the traits that had the strongest correlations individually, i.e. the plant height and RDVI indices in this case. Similar data fusion models that were investigated in previous studies varied in the ability to predict biomass over the single metric predictions and this depended on the traits that were added at different growth stages and the correlations between the traits. The integration of RGBVI and plant height resulted in small improvement in the biomass prediction in barley (*r* from 0.89 to 0.92) but no improvement in the biomass prediction was found with the integration of plant height and other VIs derived from visible and near-infrared spectra (Bendig et al., 2015). This can probably be explained by the moderate to high correlations between the plant height and various VIs found in this study (Table 2.3).

Further work will be needed to improve biomass prediction through the inclusion of additional morphological traits such as stalk diameter and additional or customized spectral bands. Some other traits that were not included in this study also showed ability to increase the estimation accuracy when combined with some of the UAS-derived traits in this study. When adding manually measured stem diameter on the UAS-derived plant height, the biomass prediction using a volumetric cylinder equation in corn was significantly improved (*r* from 0.56 to 0.93) (Varela et al., 2017). However, automating

This chapter was published on *Frontiers in Plant Science*: doi: 10.3389/fpls.2018.01406

stem diameter measurements is challenging and may not be useful in many energy sorghum varieties that do not flower in North America (SD Kresovich, personal communication). Another case would be the combination of hyperspectral canopy reflectance and plant height which improved the accuracy of estimating winter wheat biomass (*r* from 0.73 to 0.91) (Yue et al., 2017). In addition, customization of spectral bands of the UAS-based multispectral sensor based on the feature spectral bands derived from the leaf-level or ground-based hyperspectral sensing (Yendrek et al., 2017) for specific applications can scale up the throughput of phenotyping capabilities in the field while reducing the sensor instrument cost.

Improvement can also be achieved by including temporal data during the growing season and using more sophisticated statistical models. The late-season biomass predicted by single or multiple UAS-derived traits had strong exponential correlations with the sampled fresh biomass (maximum $r = 0.84$) and dry biomass (maximum $r = 0.88$); however, no significant improvement was found if multiple traits collected on the same date were used to build models (Table 2.4 and 2.5). Similar results were reported in study on sorghum biomass prediction (Z. Zhang, Masjedi, Zhao, & Crawford, 2017) showing that more data on additional traits measured on the same day provided no significant improvement for biomass prediction. However, significant improvements were found when measurements from multiple time points with either a single trait or multiple traits were used (Zhang et al., 2017). Also, the exponential relationships found between UAS-derived traits and biomass in this study were similar to a previous finding in barley (Bendig et al., 2014).

This chapter was published on *Frontiers in Plant Science*: doi: 10.3389/fpls.2018.01406

We recommend segmenting vegetation pixels and shaded soil pixels for some VI calculations to avoid the interference of shaded soil pixels in the calculations. Shadows that were cast on the canopy and soil were identified in this study to have much higher NDVI values than the sunlit vegetation pixels (Figure 2.3). If an averaged VI value was calculated for all pixels encompassed within a plot boundary, plots with more shaded vegetation and soil areas may result with higher VI values than those without much shaded areas even though the NDVI of the actual leaves may be lower. Shading may not be a problem for production agricultural applications when the whole field was planted with same variety and population; however, in the application of phenotyping when many small plots that contained different varieties or uneven stands this cause substantial errors in estimating the true canopy VIs. Accurate segmentation of sunlit vegetation and shaded vegetation and soil pixels in the image processing is important to ensure the reliability of VI values. In this study, we used the ExG index map for segmentation which was effective but still resulted with some mis-classification of shaded vegetation and shaded soil pixels. This also resulted in a lower estimation of canopy cover especially for those plots with significant shadows. Future research will be needed to investigate the hyperspectral reflectance patterns of the sunlit and shaded vegetation and soil pixels and corresponding classification algorithms with proper band selection techniques (Sun, Zhang, Du, Li, & Mark Lai, 2015) to customize multispectral cameras for high-throughput applications.

The results obtained using UAS-derived DSM to estimate plant height are very promising (r = 0.85) and are similar to other studies (Chang et al., 2017; Geipel et al., 2014; Hu et

This chapter was published on *Frontiers in Plant Science*: doi: 10.3389/fpls.2018.01406

al., 2018; Malambo et al., 2018; Pugh et al., 2018; Watanabe et al., 2017). Considering the strong correlation between the late-season plant height and the sampled fresh and dry biomass ($r >= 0.81$), this method can be used to quickly estimate plant biomass. The UAS-derived plant height in this study was only investigated using the data collected on a single date late in the season since the main purpose was end-of-season biomass prediction. The accuracy of the height estimation achieved in this study (*RMSE* = 49.8 cm) needs to be improved in order to be applied to plant height estimation in earlier growth stages when plants are smaller. Ideally, the structure from motion (SfM) algorithm used behind this technology to generate the point clouds or the structure of a targeted object can achieve reprojection error at only about one pixel (Snavely et al., 2008) which in our case would be about 1.3 cm accuracy. However, in real world agricultural applications, errors are induced due to the movement of the plant canopy by the wind (Chang, Jung, Maeda, et al., 2017). During our data collections, the wind speed was 5 m/s (10 mph) which caused the top canopy to sway at decimeter level. This rendered the SfM algorithm difficult to use because matched keypoints among images taken from different angles were hard to find and therefore errors were generated. Moreover, variation in leaf angle, canopy structure and presence or absence of panicles among genotypes caused the discrepancy between manually sampled plant height and plant height estimated from the UAS-derived point clouds data. In addition, the accuracy of UAS-derived plant height also depends on the accuracy of the derived digital terrain model (DTM) or the elevation of the field (Malambo et al., 2018). In this study, we assumed a constant elevation change of the field since the field was flat and relatively

This chapter was published on *Frontiers in Plant Science*: doi: 10.3389/fpls.2018.01406

small (1.38 ha); however, ignoring the within-field unevenness may induce a small amount of error. A pre-planting elevation mapping can largely reduce such errors.

Improving prediction accuracy to develop a more generally applicable model for energy sorghum will be a future goal. The models developed in this study were based on a single season and so they may be further improved through the incorporation of multi-season and multi environment data. Incorporating additional data sets such as growing degree days, precipitation, soil physicochemical properties, planting dates and other agronomic practices may all allow for the further improvement of predictive models using data from UAS.

2.5 CONFLICT of INTEREST

The authors certified that they have no affiliations with or involvement in any organization or entity with any financial interest, or non-financial interest, in the subject matter or materials discussed in this manuscript.

2.6 AUTHOR CONTRIBUTION

JL, AV, YS conducted the aerial data collections. DPS provided the field, all the ground truth and hyperspectral radiometer data. JL and YS performed the aerial data analysis and wrote the manuscript. DPS edited and reviewed the manuscript. All authors reviewed the manuscript and agreed with the submission.

2.7 ACKNOWLEDGMENTS

We gratefully acknowledge startup funds provided by the Agricultural Research Division and the Office of Research and Economic Development of the University of Nebraska-Lincoln, provided to Yeyin Shi, and a grant from Office of Science (BER), U.S. Department of Energy, Grant no DE-SC0014395 to Daniel Schachtman.

In addition, the authors wish to thank Stephanie Futrell and Bert Devilbiss who were involved in the field ground truth data collection, lab analysis and hyperspectral data collection and analysis and the laboratories of Dr. Stephen Kresovich (Clemson) and Dr. Ismail Dweikat (UNL) who provided seed for these experiments.

This chapter was published on *Frontiers in Plant Science*: doi: 10.3389/fpls.2018.01406

CHAPTER 3 PRINCIPAL VARIABLE SELECTION TO EXPLAIN GRAIN YIELD VARIATION IN WINTER WHEAT FROM UAV-DERIVED PHENOTYPIC TRAITS

Jiating Li[1], Madhav Bhatta[2], Nicholas D. Garst[2], Hannah Donoho[2], Arun-Narenthiran Veeranampalayam-Sivakumar[1], P. Stephen Baenziger[2], Vikas Belamkar[2], Reka Howard[3], Yufeng Ge[1], Yeyin Shi[1*]

[1]Department of Biological Systems Engineering, University of Nebraska-Lincoln, Lincoln, NE, USA, [2]Department of Agronomy and Horticulture, University of Nebraska-Lincoln, Lincoln, NE, USA, [3]Department of Statistics, University of Nebraska-Lincoln, Lincoln, NE, USA

*** Correspondence:**

Name: Yeyin Shi

Email: yshi18@unl.edu

ABSTRACT

Automated phenotyping technologies are constantly advancing. However, collecting diverse phenotypic traits throughout the growing season and processing massive amounts of data still take lots of efforts and time nowadays. Selecting minimum number of phenotypic traits that have the maximum predictive power has the potential to largely reduce the phenotyping efforts. The objective of this study was to select principal UAV-derived phenotypic traits (vegetation index and plant height) on winter wheat along the growing season that contribute most in explaining grain yield. The experiment field located in Lincoln of Nebraska, USA, where ten winter wheat check lines with 17 replicated plots per line were randomly distributed over the field as part of a larger augmented design for yield trail. Five times of multispectral imagery and seven times of

This chapter was prepared for journal submission

RGB imagery were collected by an UAV system during the spring growing season in 2018. Grain yield was sampled at the end of season (early July). From multi-temporal UAV-derived vegetation index (VI) and plant height maps, a total of 172 parameters was calculated for each plot including statistical descriptions of the pixel values and the dynamic growth rate. These variables were considered as candidates in two variable selection algorithms: LASSO regression (the least angle and shrinkage selection operator) and random forest. The regression coefficients estimated by LASSO or the permutation importance from random forest of each variable was used as importance score for variable selection. And 10 variables with highest averaged importance scores were selected by each algorithm, respectively. Results showed that most of the selected variables were derived from plant height map, especially related with the plant height measured in the last two data collections in the growing season (grain filling and maturity stages). The capability of using the selected principal variables on yield prediction was also investigated with the ridge regression and support vector machine (SVM) models. The selected principal variables exhibited similar predictive power on grain yield compared with the prediction result using all 172 variables on the testing data set. The methods provided in this study can be applied to larger data set collected from multiple years and locations to narrow down the important phenotypic traits and growth stages to be focused on in the data collection and processing to streamline the breeding process.

Key words: unmanned aerial vehicle, phenotyping, yield prediction, lasso, random forest, ridge regression, SVM

This chapter was prepared for journal submission

3.1 INTRODUCTION

As one of the main source for overall food production, wheat has the highest hectarage over the world (Belamkar et al., 2018; Makino, 2010). Boosting grain yield to feed the ever growing world population is one of the major focuses in wheat breeding (Foley et al., 2011; Godfray et al., 2010; Ray, Mueller, West, & Foley, 2013). This requires evaluating and screening large number of genotypes in field under various environments (Araus & Cairns, 2014). Recently developed high-throughput field-based plant phenotyping (HTPP) technology provides rapid and efficient screening on large amounts of crop lines (Araus et al., 2018).

Various sensing technologies are available nowadays for HTPP and massive amount of data can be generated throughout the growing season. Handheld sensors are not typically considered as high-throughput method but are widely used in breeding programs (Aparicio, Villegas, Casadesus, Araus, & Royo, 1999; Bandyopadhyay et al., 2014; Das, Mishra, & Kalra, 1993; Ferrio et al., 2005; Prasad et al., 2007; Serrano, Filella, & Penuelas, 2000). A handheld spectroradiometer that measures leaf or crop canopy reflectance with a few wide spectral bands or hundreds of narrow spectral bands can generate kilobytes to megabytes of point measurement data in a field. Recently advances in ground-based and aerial-based mobile platforms provide large sensor payloads and throughputs both spatially and temporally; thus, generating significantly more volume of data. For example, a multi-sensor cart was developed for soybean and wheat breeding (Bai, Ge, Hussain, Baenziger, & Graef, 2016), mounted with ultrasonic sensor, NDVI sensor, thermal infrared radiometer, spectrometer, RGB sensor, as well as other ancillary

sensors. Similar platforms include ‘phenocart’ (Crain, Reynolds, & Poland, 2017), mobile ‘PhenoTrac’ (Kipp, Mistele, & Schmidhalter, 2014; Rischbeck et al., 2016), and tractor-based semi-automatic system (Comar et al., 2012). As for the aerial-based platforms, the unmanned aerial vehicle (UAV) is nowadays gaining increased interests due to the easiness to operate, high spatial resolution, and quick coverage (Benincasa et al., 2018; Geipel et al., 2016; Guan et al., 2019; Haghighattalab et al., 2017). Typical sensors equipped by UAVs in agricultural applications are RGB cameras (Du & Noguchi, 2017), multispectral cameras (T. Duan et al., 2017a), thermal camera (Kefauver et al., 2017b), and hyperspectral camera (Kanning et al., 2018). Multiple phenotypic traits are available from these sensors, including spectral traits such as vegetation indices and canopy temperature, morphological traits such as plant height, stand count and canopy ground cover, as well as the dynamic change indicating the growth or senescence rate. The raw data collected by the UAVs are usually in the image format in large data size. Take this study as an example, an approximate storage of 30-gigabyte data (around 9000 multispectral images and 1000 RGB images) was collected in one-time flight over the 3-acre research field. Such flights can be conducted in a weekly basis throughout the growing season.

In terms of grain yield modeling, a general idea is to extract vegetation indices (T. Duan et al., 2017a; Hassan, Yang, Rasheed, Yang, et al., 2018; Kyratzis, Skarlatos, Menexes, Vamvakousis, & Katsiotis, 2017)or morphological traits as predictors (Moravec et al., 2017). For example, normalized difference vegetation index (NDVI) derived from UAV imagery on each growth stage correlated well with wheat grain yield, with the highest

correlation appeared around flowering time (r = 0.91) (T. Duan et al., 2017a). In addition to using single-stage derived phenotypic traits, researchers also attempted to exploit extra predictive power by integrating phenotypic traits from multiple growth stages. In the study of Du & Noguchi (Du & Noguchi, 2017), five accumulative RGB indices over eight flights were used as variables in stepwise regression models, resulting in a best model with four indices selected (r = 0.69 on validation set). Additionally, Haghighattalab et al. (Haghighattalab et al., 2017) input multi-temporal phenotypic traits into principal component regression and geographically weighted (GW) model to estimate wheat yield. The GW model considered spatial relationship in acquired images, resulting in better predictive performance on grain yield (r = 0.74/0.46 for drought/irrigated environments).

Studies found that using multiple-stage phenotypic traits together had the tendency to outperform using single-stage data in grain yield prediction (Montesinos-López et al., 2017; Laigang Wang, Tian, Yao, Zhu, & Cao, 2014). It is a positive finding in terms of enhancing grain yield predictive power. However, when the objective is to obtain better interpretation between individual phenotypic trait and grain yield, the predictive model using all phenotypic traits might be too complicated. In order to derive better understanding of individual phenotypic trait's contribution, in the meantime, retaining the advantage of using multiple-stage phenotypic traits, a prospective method is to add variable selection procedure into modeling. This methodology has already been adopted by Du & Noguchi (Du & Noguchi, 2017), as mentioned above, the stepwise regression acted as both predictive model and variable selection algorithm.

This chapter was prepared for journal submission

Variable selection is a process of selecting variables based on individual variable's predictive power for responsive variable (Degenhardt, Seifert, & Szymczak, 2017). It has the potential to reduce computational complexity and improve data analysis efficiency by providing more effective variables and better data understanding (Andersen & Bro, 2010; Guyon & Elisseeff, 2011). In this study, two common selection methods were adopted: LASSO regression and random forest. LASSO was firstly proposed by Tibshirani in 1996 (Tibshirani, 1996). It puts penalty on variables so that some of the near-zero regression coefficients will be estimated exactly as zero, thus removing them out from the selection result. It is feasible when the number of variables larger than the number of observations (Leng, Lin, & Wahba, 2006; C. H. Zhang & Huang, 2008). Random forest (Breiman, 2001) aggregates hundreds of individual decision trees to achieve better trade-off between bias and variance (Genuer, Poggi, & Tuleau-Malot, 2010; Gregorutti, Michel, & Saint-Pierre, 2017). It is a ranking based nonparametric selection algorithm (Archer & Kimes, 2008; Genuer et al., 2010), providing importance measurement of individual variable. Similar to LASSO, random forest is also applicable when the number of variables is greater than the number of observations (Grömping, 2009), and it is not sensitive to the multi-collinearity issue (Li'ai Wang, Zhou, Zhu, Dong, & Guo, 2016).

To the best knowledge of the authors, only few studies conducted variable selection on UAV-derived phenotypic traits for wheat grain yield (Du & Noguchi, 2017; Haghighattalab et al., 2017). Furthermore, in these studies, only statistical descriptions of the phenotypic trait (e.g. vegetation index) map were extracted as candidates in variable selection. Considering the multi-temporal property of UAV acquired imagery, it is

meaningful to examine the predictive power of other type of variables, such as growth rate. To this end, the objective of this study was to select principal phenotypic variables that contribute most in explaining the grain yield in winter wheat, to potentially reduce the efforts in field phenotyping data collection and following data processing. Two specific objectives were:

1) To extract two types of variables from UAV-derived VI and plant height maps including statistical descriptions from map on single growth stage, and dynamic growth rate from maps on two continuous growth stages.
2) To perform principal variable selection from extracted variables, and evaluate prediction power on grain yield using the selected principal variables.

3.2 MATERIALS and METHODS

3.2.1 Field Layout

The studied field was located in Lincoln, Nebraska, USA (N 40.8581, W 96.6157), where winter wheat were grown in the growing season from the end of October, 2017, to the early July, 2018. As part of a larger augmented design for yield trail, 10 check lines (TAM304, TAM114, TAM113, Freeman, Ruth, Robidoux, WB Cedar, WB Grainfield, SY Wolf, and Gallagher) with 17 replications, in total 170 plots, were used in this study (Figure 3.1). The rest plots in this trail were reserved proprietary lines at the time of this study. Grain yield of the 170 plots was manually measured after harvest in early July.

This chapter was prepared for journal submission

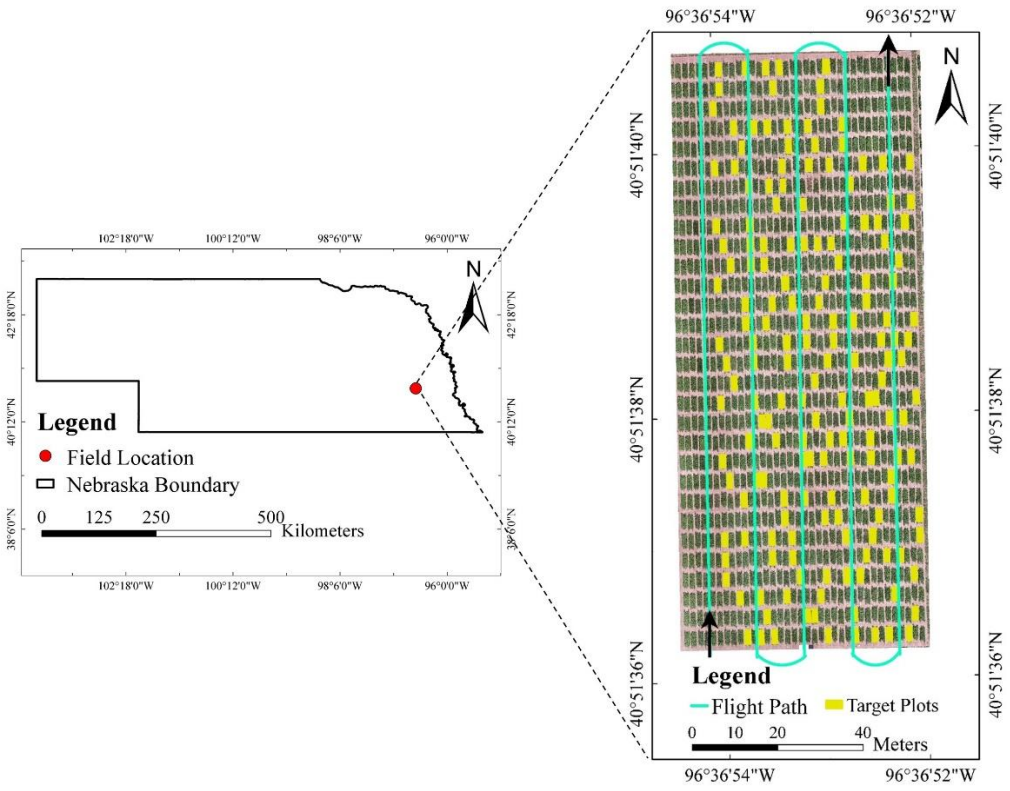

Figure 3.1. Field location and target experimental plots. Field map was collected on May 7th 2018.

3.2.2 UAV System and Flight Missions

The UAV system used in this study consists of a DJI Matrice 600 Pro multi-rotor platform (DJI, Shenzhen, China), a Zenmuse X5R RGB camera (DJI, Shenzhen, China), and a five-band multispectral camera RedEdge (Micasense, Seattle, UAS). Each individual RGB image has an effective pixel size of 4608 by 3456, and each individual multispectral band has an effective pixel size of 1280 by 960. The multispectral camera also comes with a standard calibration panel, which was imaged on ground right before or after each flight for radiometric calibration during image stitching stage.

This chapter was prepared for journal submission

Seven RGB image sets and five multispectral image sets were acquired from mid-April to mid-June in 2018, the corresponding growth stages and other details as shown in Table 3.1. Test flights were conducted before data collection, aiming at finding an appropriate flight height that can result in clearly recognizable plants in image as well as enough overlaps for image stitching. Afterwards, the flight altitude was set as 20 meters above ground level, and the forward and sideward overlaps were both set as 88%. The corresponding ground sampling distance (GSD) were around 0.5 cm/pixel for RGB stitched image and 1.35 cm/pixel for multispectral stitched image. Before each flight mission, 21 ground control points (GCP) using black and white cross-centered wooden boards were randomly distributed in the field. GPS information of these GCPs that used in geometric calibration were measured by a survey grade GNSS RTK GPS receiver (Topcon Positioning Systems, Inc., Tokyo, Japan), with sub-centimeter accuracy in X and Y directions, and centimeter accuracy in Z direction.

Table 3.1. Flight missions and corresponding growth stages.

Flight time	Acquired image type	Day of year	Growth stage
April 22nd	RGB	111	Tillering stage: Feekes 3
April 27th	RGB and Multispectral	116	Green-up stage: Feekes 5
May 7th	RGB and Multispectral	126	Jointing stage: Feekes 6
May 15th	RGB	134	Flag leaf stage: Feekes 8
May 21st	RGB and Multispectral	140	Boot stage: Feekes 9
June 1st	RGB and Multispectral	151	Grain filling: Feekes 10.5.3
June 18th	RGB and Multispectral	168	Physiological maturity: Feekes 11

3.2.3 Generate Vegetation Index and Plant Height Maps

The vegetation index (VI) and plant height maps were generated from stitched multispectral and RGB images. The image stitching was done in Pix4Dmapper (Pix4D, Lausanne, Switzerland). Other than stitched RGB or multispectral image, a digital surface

model (DSM) map were also exported along with RGB stitched map. DSM was later used to generate plant height map. More details regarding the stitching procedure can be found in Li, Shi, Veeranampalayam-Sivakumar, & Schachtman (2018).

Before generating plant height map, one necessary step was to derive digital terrain model (DTM). DTM map represents the elevation of soil surface. In this study, the DTM was created by interpolation among soil points that were sampled after soil segmentation. Specifically, RGB stitched image from the earliest flight (it had largest area of bare soil surface) was transferred into (CIE) L*a*b* color space (MATLAB R2018b, the MathWorks, Inc. USA), among which the distribution of a* channel is generally considered as a Gaussian-mixture model of vegetation pixels and soil pixels (L. Li et al., 2018). According to the threshold calculation method described in Y. Liu, Mu, Wang, & Yan (2012), a raster with only soil pixels was created by setting vegetation pixels (pixel value smaller than threshold value) as null value. From this raster, thousands of soil points were randomly sampled using Fishnet tool, and were then used to create DTM by Kriging interpolation tool in ArcMap 10.5.1 (Esri Inc. CA, USA). Thereafter, the plant height map was calculated by subtracting the elevation in DTM map from the elevation in DSM map.

VI (NDVI, GNDVI, and NDRE) maps were obtained using the stitched 5-band spectral images in RStudio 1.0.153 (RStudio, Inc. Boston, USA), according to the following equations (1-3). NDVI (normalized difference vegetation index) is the most frequently used index in UAV-based wheat yield monitoring (T. Duan, Chapman, Guo, & Zheng, 2017b; Guan et al., 2019; Hassan, Yang, Rasheed, Yang, et al., 2018). Other than NDVI,

green NDVI (GNDVI) was found to be the most correlated VI with grain yield among the other investigated indices (Kyratzis et al., 2017). Normalized difference red edge (NDRE), as a good estimator for leaf chlorophyll, was found to be efficient in explaining the variance of leaf area dynamics or senescence patterns of ten sorghum genotypes (Potgieter et al., 2017).

$$NDVI = (R_{NIR} - R_{Red})/(R_{NIR} + R_{Red}) \quad (1)$$

$$GNDVI = (R_{NIR} - R_{Green})/(R_{NIR} + R_{Green}) \quad (2)$$

$$NDRE = (R_{NIR} - R_{Red-edge})/(R_{NIR} + R_{Red-edge}) \quad (3)$$

where *R* stands for the reflectance value for each spectral band, the spectral band was indicated in the subscript.

In order to conduct parameter extraction on the level of experimental plot, a prerequisite step was to delineate plot boundaries (ArcMap). Experimental plots were equally delineated by a rectangular boundary (Figure 1) and was assigned with a specific ID. The created shape file was then used as shape mask for calculating different parameters from VI or plant height map.

3.2.4 Description of Variables Extracted from VI and Plant Height Maps

To extract representative variables directly from UAV phenotypic trait map, a common and timely efficient way was to calculate individual variable for each experimental plot. Such as maximum or mean of VI (Hunt et al., 2010; Schirrmann et al., 2016; Shafian et al., 2018), mean or percentiles of plant height (Bendig et al., 2014; Chu et al., 2016; Holman et al., 2016; Iqbal, Lucieer, Barry, & Wells, 2017; Schirrmann et al., 2016). However, given the spatial property of imagery, representing the whole plot using single

variable tends to be biased. Other potential useful information might be ignored in this situation.

To this concern, the first type of variables was statistical descriptions for the pixel values in each VI or plant height map. Based on original map, trimmed mean (mean value after trimming top and bottom 10% values), median (equals to 50^{th} percentile), mode, and standard deviation were derived for plot in VI maps; similarly, trimmed mean, median, 95^{th} percentile, and standard deviation were derived for plot in plant height maps. By transferring each original map into a gray-level co-occurrence matrix (GLCM), another four statistical variables were calculated to describe map texture. The GLCM is a feature extraction method, from which the second-order statistical texture parameters could be derived (Mohanaiah, Sathyanarayana, & Gurukumar, 2013). The second-order means that GLCM only considers the relationship between two pixels. The four second-order statistical variables derived from GLCM were contrast, correlation, energy, and homogeneity. Contrast represents the local gray level variations in an image; high contrast indicates any exist of edges, noise, or winkled texture. Correlation measures the linear dependency of specified pixel pairs. Energy, also known as angular second moment, sums up the squared elements in GLCM; image with higher energy has better homogeneity. As for homogeneity, it is also called inverse difference moment and stands for the local homogeneity; high value represents uniform local gray level.

The second type of variables was dynamic growth rate, representing winter wheat seasonal growth by using multi-temporal data. Although many UAV studies on winter wheat conducted multiple UAV flights over season, few of them considered the

correlation between dynamic growth rate and grain yield. Instead, the common method was to correlate spectral data with grain yield at single growth stage. To the knowledge of the authors, among UAV studies on winter wheat, only Du & Noguchi (2017) accumulated CVI over time (Du & Noguchi, 2017) and Haghighattalab et al. (2017) gathered multiple-time VIs together for the wheat grain yield estimation (Haghighattalab et al., 2017). Different from these two studies where phenotypic traits were combined together, this study subtracted information between two continuous data collections to derive growth rate. Taking NDVI dynamic curve as an example (Figure 3.2), the growth rate was defined as the slope between continuous NDVI values (trimmed mean). Since NDVI dynamic curve connected five time points, four growth rates were calculated. Correspondingly, with seven time points in plant height dynamic curve (Figure 3.5(B)), six growth rates were calculated for plant height.

Among the first type of variables, trimmed mean was found to highly correlate with median value. Therefore, the trimmed mean value was only used to calculate dynamic growth rate, but was not counted as candidates in variable selection. Summing up all different types of parameters, there were finally 172 variables for each experimental plot, which were summarized in Table 3.2.

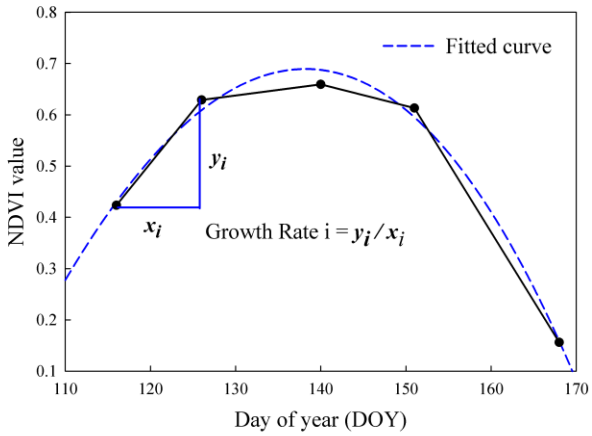

Figure 3.2. Define growth rate calculated from dynamic VI or plant height curve.

Table 3.2. Summary of the 172 variables extracted from VI and plant height maps.

Phenotypic trait map	**Times of data collections**	**Number of variables**	
		Statistical descriptions	**Dynamic growth rate**
Plant height	Seven	49	6
NDVI	Five	35	4
NDRE	Five	35	4
GNDVI	Five	35	4
Total number of parameters			**172**

3.2.5 Principal Variable Selection for Grain Yield Estimation

The 172 variables mentioned above were treated as candidates in variable selection for explaining grain yield variations. These variables were normalized before selection by LASSO and random forest.

The main parameter tuned in LASSO was lambda, a shrinkage penalty term. It was tuned through 10-fold cross validation, with mean squared error (MSE) as loss function. Lambda shrank some variable coefficients to zero, allowing non-zero variables selected. Other than selection, LASSO also estimated the regression coefficients for selected variables. Since all variables were normalized beforehand, variable with higher absolute

coefficient could be considered to contribute more for grain yield. Therefore, the absolute regression coefficient was used as importance score for the variable selected by LASSO.

Random forest considers the ranking of permutation importance of variables. Generally, if a variable X is importance for the dependent variable Y, permuting the order of X will break the correlation link between X and Y, thus increasing prediction error (MSE) (Gregorutti et al., 2017). That is, the higher increase in MSE of a variable X is, the more important that variable is. Therefore, the increase in MSE (%IncMSE) was considered as importance score in random forest selection. Parameter tuned for random forest in this study was the number of trees to grow and number of variables randomly sampled as candidates at each split, which were optimized by grid search as 1500 and 2 separately.

Considering the instable results from most variable selection methods (Gregorutti et al., 2017), each algorithm was set to ran 30 times with different random seeds. Afterwards, each variable would have two lists of importance scores, with the length of 30, from LASSO and random forest. To finally determine the most important variables, the top 10 variables with the highest averaged importance scores were chose for LASSO and random forest separately.

To evaluate selected variable set on explaining the variations in grain yield, ridge regression and support vector machine (SVM, non-parametric) with Gaussian kernel were applied. Ridge regression is a parametric algorithm for prediction. It has the ability of addressing the collinearity issue that was not handled by multiple linear regression (de Vlaming & Groenen, 2015; McDonald, 2009; Orhan, Eyduran, Tatliyer, & Saygici, 2016). SVM is based on statistical learning theory, and is known with good performance

on handling highly non-linear data (Hultquist, Chen, & Zhao, 2014). The version of SVM used in regression problem was introduced by Vapnik in 1997 (Vapnik, Golowich, & Alex, 1997). 170 observations were split into 80% as training data and 20% as testing data for ridge regression and SVM model. Comparisons were made based on performances on testing data: between LASSO selected 10 variables and all 172 variables, as well as between random forest selected 10 variables and all 172 variables. Correlation coefficient (*r*) and root mean squared error (*RMSE*) were the evaluative parameters.

3.3 RESULTS

3.3.1 Growth Dynamic in terms of VI and Plant Height

Multi-temporal maps of plant height, NDVI, NDRE, and GNDVI were presented in Figure 3.3. In VI maps, greener pixel indicated higher wheat crop vigor; in plant height maps, the greener means higher wheat plant. It is observable that, the plant height maps showed an increasing trend over growth stages. While all three VI maps indicated that the wheat had the highest vigor on the 140 DOY (the 140^{th} days of year, corresponding to the middle of data collections), and a significant drop appeared after the 151 DOY. The fact that most of the wheat plots turned yellow around the 168 DOY could explain the significant low value in VI maps.

A quantitative way to describe growth dynamics was showed in VI or plant height dynamic curves (Figure 3.4). The dynamic curve values were trimmed mean for VI and

the 95th percentile for plant height. As illustrated in Figure 3.4 (A), NDVI, GNDVI and NDRE followed similar growth trend that reached peak at the middle time point, with a significant drop after the 151 DOY. It also exhibited the different growth rates over season. For example, NDVI had almost equal growth rates between the 116 and 140 DOYs, whereas NDRE and GNDVI had slight increase between the 116 and 126 DOYs but significant increase between the 126 and 140 DOYs. In Figure 3.4 (B), the plant height dynamic showed an increasing trend along seven data collections, with slight increase between last two dates. Both trends were similar to those illustrated in Figure 3.3.

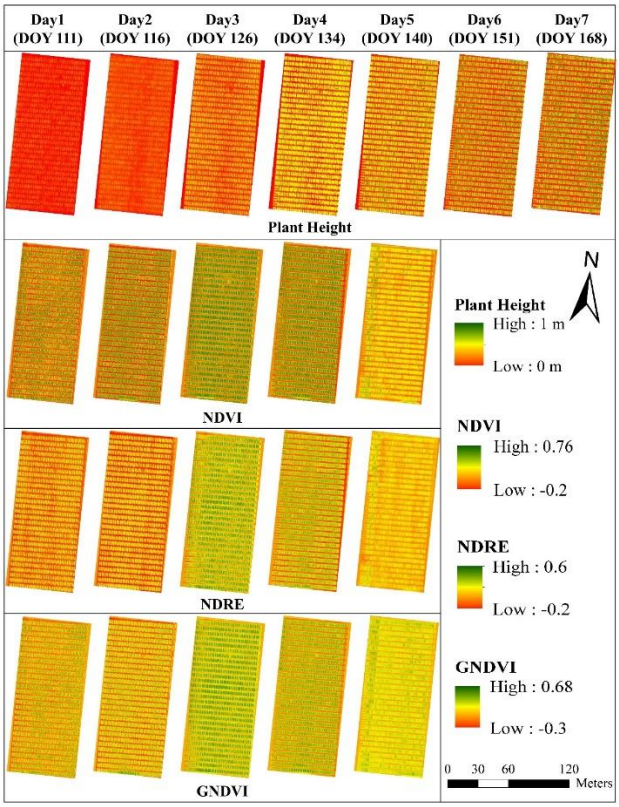

This chapter was prepared for journal submission

Figure 3.3. Processed VI and plant height maps, over multiple collection dates. DOY represents 'day of year' for each date, corresponding to x axis in Figure 5.

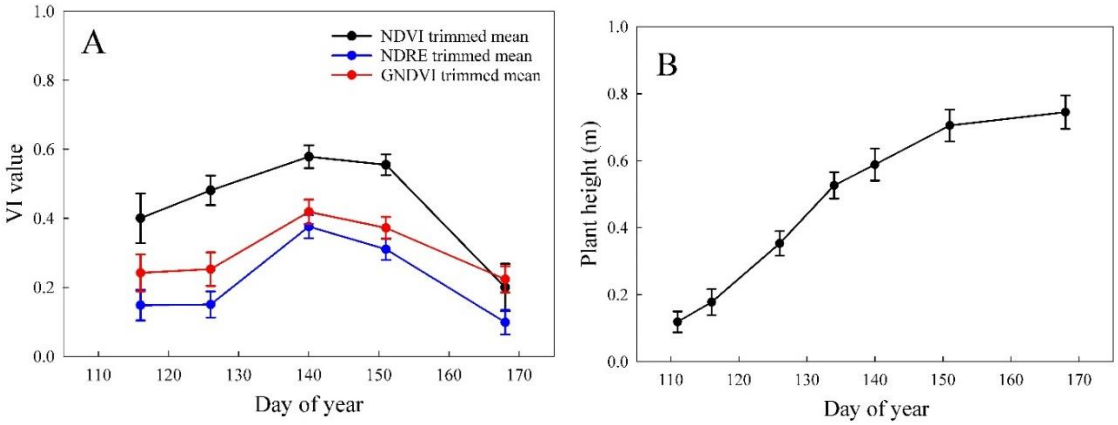

Figure 3.4. Growth dynamic in terms of UAV-derived VIs and plant height over the days in 2018. Bars on each date show the standard deviation of the 170 plots.

3.3.2 Variable Selection by LASSO and Random Forest

After 30 random runs, the top 10 variables with highest averaged importance scores were determined for LASSO and random forest separately (Figure 3.5). Naming of variable in Figure 3.5 explained the information on types of phenotypic traits and times of data collection. In LASSO selected variable set, the parameter extracted from plant height map on seventh data collection (e.g. PH.Day7.Para1) had the highest averaged importance score. Furthermore, eight out of the 10 variables related to plant height. As for the random forest selected variable set, the parameter extracted from plant height map on sixth data collection (e.g. PH.Day6.Para1) showed the highest averaged importance score. Seven out of 10 variables were extracted from plant height maps.

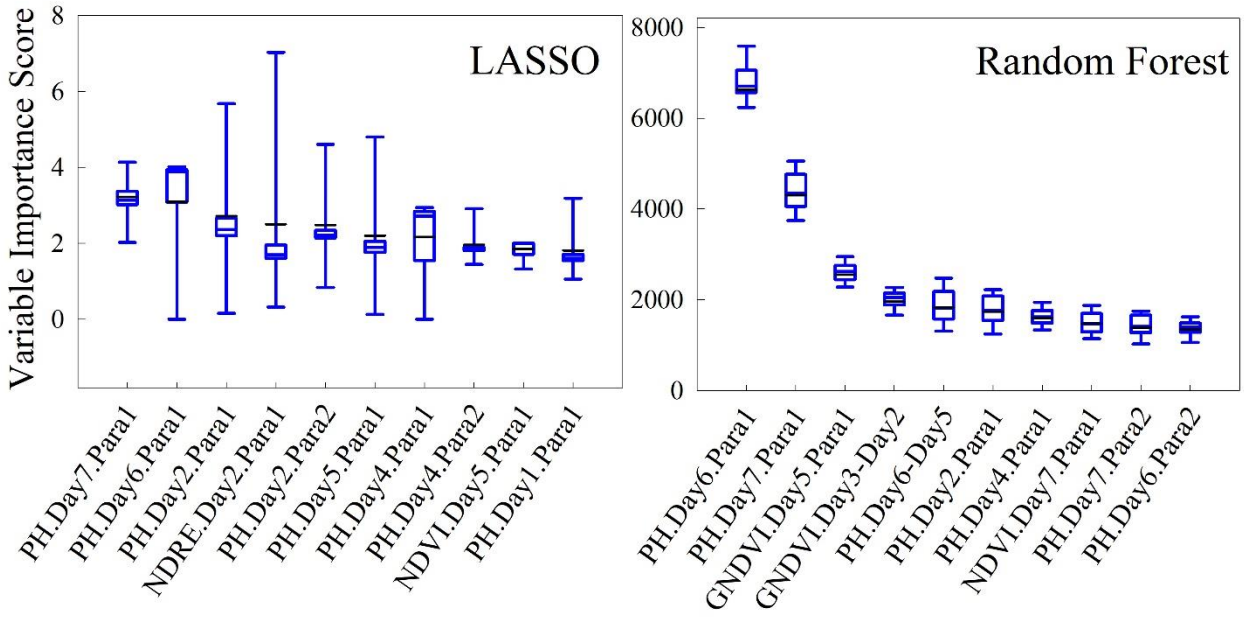

Figure 3.5. Top 10 variables with highest averaged importance score, from LASSO and random forest respectively.

* Examples on reading variable names: PH.Day7.Para1, meaning one parameter from plant height map on the seventh data collection. PH.Day7.Para2 means another parameter from plant height map on the seventh data collection. GNDVI.Day3-Day2, indicating the dynamic growth rate calculated between Day2 and Day3 data collections.

3.3.3 Explain Grain Yield using Selected Variable Sets

Using the two variable sets determined above, the grain yield was explained in both ridge regression and Gaussian kernel based SVM model. Performances on testing data (20%, 34 plots) were reported in Table 3.3. With ridge regression, LASSO selected variable set had relatively higher performance (r = 0.41±0.12, RMSE = 302±31) than using all 172 variables (r = 0.37±0.11, RMSE = 306±33), whereas variables determined from random forest resulted in similar performance (r = 0.36±0.10, RMSE = 308±34) with using all variables. As for the SVM model, performance of variable set from either LASSO (r =

0.29±0.16, RMSE = 334±30) or random forest (r = 0.39±0.11, RMSE = 311±36) was slightly lower than that using all available variables (r = 0.41±0.13, RMSE = 302±29).

To better depict the relationship between measured grain yield and estimated grain yield, scatter plots with results from testing data were provided in Figure 3.6. The first row of sub-figures (Figure 3.6 (A-C)) corresponded to using ridge regression as predictive model, and the second row (Figure 3.6 (D-F)) related to SVM predictive model. Each column represented one type of variable set: LASSO selected variable set, random forest selected variable set, and all 172 variable set (from left to right). It observable that the predicted grain yield by ridge regression was less scattered than that by SVM model.

Table 3.3. Performance on explaining grain yield variations in testing data, using variable sets determined from LASSO and random forest, as well as all available variables.

Variable	**Ridge regression**		**SVM with Gaussian kernel**	
	r	**RMSE (g/plot)**	**r**	**RMSE (g/plot)**
10 variables selected by LASSO	*0.41±0.12	302±31	0.29±0.16	334±30
10 variables selected by random forest	0.36±0.10	308±34	0.39±0.11	311±36
All 172 variables	0.37±0.11	306±33	0.41±0.13	302±29

* mean ± standard deviation

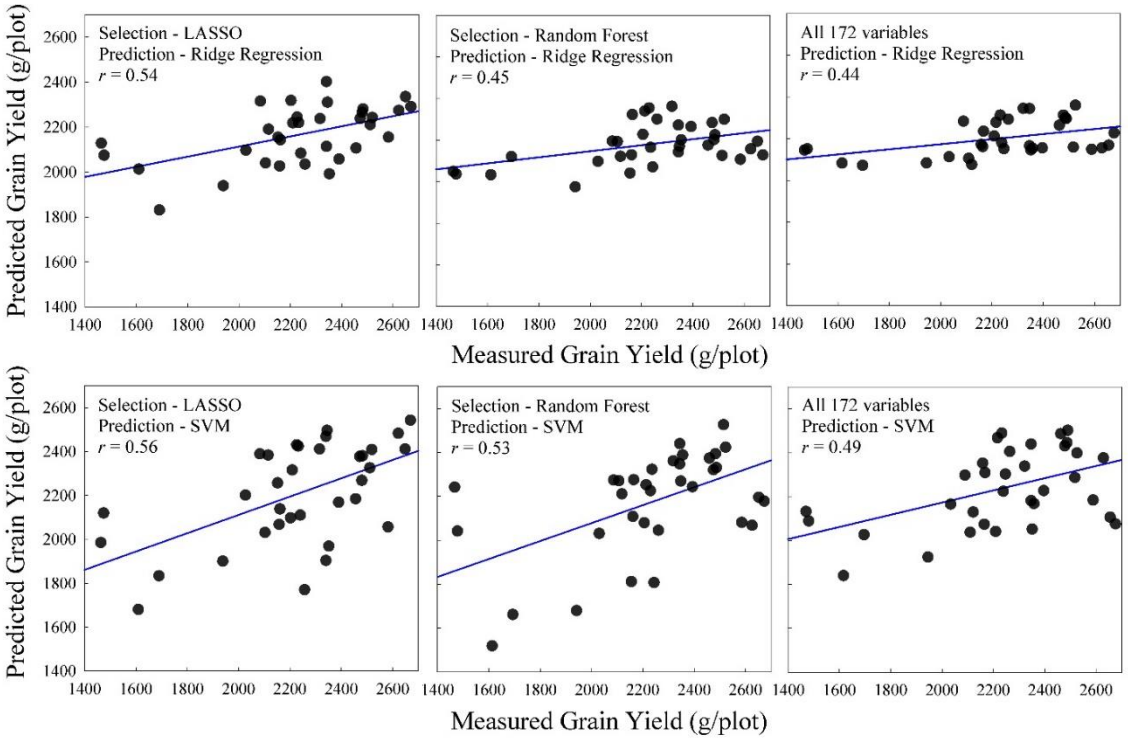

Figure 3.6. Relationship between measured and estimated grain yield from different predictive models (ridge regression and SVM) and different variable sets (LASSO selected, random forest selected, and all 172 variables).

3.4 DISCUSSIONS

The processed VI and plant height maps (Figure 3.3) showed similar growth trends with those in corresponding dynamic curves (Figure 3.4): VI reached peak value around May 21 (boot stage) and plant height kept increasing until June 18 (physiological maturity). The seasonal changes of three VIs were similar to each other, which were typical and have already been found in relative studies (Comar et al., 2012; Kalubarme, Potdar, Manjunath, Mahey, & Siddhu, 2003). The growth trend of plant height was also typical, similar to the trend of sigmoid curve (Chang, Jung, Maeda, et al., 2017; Chu et al., 2016). These could be positive evidences for the feasibility of applying UAV on wheat growth

monitoring. It was also noticeable that VI curves started to drop around May 21, whereas the growth rate of plant height decreased significantly after June 1. Considering the flowering date that was manually recorded (from end-May to early-June), it is possible that these symptoms, e.g. vigor starting to drop and height growth rate starting to decrease, were correlated with flowering.

Looking at the selection results by LASSO and random forest (Figure 3.5), the results in random forest were more consistent than that in LASSO. This was most likely caused by multi-collinearity issue among variables. For example, some variables might come from the same day, or calculated from the same phenotypic trait maps. The collinearity issue affected more on LASSO than on random forest, since there were larger deviations for each variable's importance scores in LASSO (Figure 3.5). When there are correlated variables, LASSO would arbitrarily select only one from the correlated variable group, thus resulting in inconsistent selections (Lu & Petkova, 2014). To alleviate the effect, the solution adopted in this study was to randomly run the algorithm for 30 times, and to summarize from 30 sets of selection results. Another possible solution that could be considered as future work is, to cluster correlated variables into group first and do selection on representative variables later (Bondell & Reich, 2008; Bühlmann, Rütimann, van de Geer, & Zhang, 2013). This alternative solution would not only provide better understandings of the underlying relationship among variables, but also allow us to know which group of variables are more important.

Although the selection results in LASSO and random forest were not exactly the same, both algorithms agreed on two findings. Firstly, both the top two variables were related to

plant height from last two collection dates (grain filling and physiological maturity stages). Compare to earlier data collections, the last two collection dates were more close to final grain yield sampling date (early July). This could be a possible reason for the higher importance of later season plant height. Grain filling stage has already proved to be critical for assessing wheat grain yield in other related research (Bowman et al., 2015; Hassan, Yang, Rasheed, Jin, et al., 2018; Laigang Wang et al., 2014). If the importance of later season plant height were further confirmed, it would be much helpful for decision making on final grain yield harvesting, especially when there were limited time or cost for harvesting.

Furthermore, both LASSO and random forest selection results agreed that most of the selected variables were derived from plant height maps. It probably indicated that, compare to spectral index, plant height might be more essential in explaining the variations in wheat grain yield. In fact, the relationship between plant height and wheat yield has always been an interesting topic for breeders. Early back in 1978, Law (Law, Snape, & Worland, 1978) found a positive relationship between plant height and wheat yield. Further, with wheat plant height measured over multiple growth stages, strong positive correlations were found between plant height and final grain yield (Girma et al., 2006). However, the correlation was not always positive. In the study of Khan (2010) (Khan, Azam, & Ali, 2010), plant height was negatively correlated with grain yield. A reasonable explanation for the negative correlation in this study was lodging of high plants. Although the correlations were not consistently positive or negative, the existence of correlation between plant height and wheat grain yield was still conformed. This

conclusion would have great significance in the case when only plant height measurement was available for wheat grain yield estimation.

When using selected top ten-variable sets to estimation grain yield, comparable performances were obtained with using all 172 variables, either by ridge regression or by SVM model. It is reasonable to state that, in this study, using more variables does not necessary significantly improve the estimation performances on grain yield. Rather, reduced number of variables could achieve comparable performances. However, given the limited number of wheat lines studied, this statement might not be true in other cases. It needs further investigation by using more wheat lines under varied environmental conditions.

3.5 CONCLUSIONS

By extracting three types of features (statistical, texture, dynamic) from UAV-derived VIs and plant height maps, this study applied two variable selection methods (LASSO, random forest) to select principal variables for winter wheat final grain yield estimation. Both LASSO and random forest selection results showed that plant height, especially during later growth stages (grain filling and maturity), had relatively higher importance score for explaining grain yield. Furthermore, selected variable sets resulted in satisfactory performance on estimating grain yield, with r ranging from 0.13 to 0.53 in ridge regression or SVM model.

This chapter was prepared for journal submission

Given the results from this single-year data with limited wheat lines, the proposed variable selection procedure could possibly be adopted in further studies with more wheat lines and varied environmental conditions or locations. This allows more confidence to draw conclusions, and thus providing potentials for saving efforts on either phenotyping data collection or data processing.

3.6 CONFLICT of INTEREST

The authors certified that they have no affiliations with or involvement in any organization or entity with any financial interest, or non-financial interest, in the subject matter or materials discussed in this manuscript.

3.7 AUTHOR CONTRIBUTION

JL, AV, YS conducted the aerial data collections. VB, NDG, HD, MB, and PSB provided the field, all the ground truth and hyperspectral radiometer data. RH and YG helped editing the manuscript. JL and YS performed the aerial data analysis and wrote the manuscript. All authors reviewed the manuscript and agreed with the submission.

CHAPTER 4 CONCLUSIONS AND FUTURE WORK

Benefit from the advancing UAV technique, it is getting easier and more efficient to screen high-throughput phenotypic data. In this study, crop phenotypic traits were derived from UAV-collected RGB imagery and five-band multispectral imagery. These traits consisted of morphological feature (e.g. canopy cover and plant height) and spectral feature (e.g. vegetation index). The goal was to exploit the potential of using UAV-obtained phenotyping information on evaluating agronomic or physiological traits (e.g. biomass, yield) in sorghum and winter wheat.

Simple and multiple exponential regression models were established for sorghum biomass estimation using the derived morphological and spectral traits. Results showed that, the UAV-derived plant height was strongly correlated with manually measured plant height ($r = 0.85$); and the estimated biomass using plant height, canopy cover and VIs had strong correlations with the sampled biomass of fresh stalks and leaves (maximum $r = 0.85$) and the biomass of dry stalks and leaves (maximum $r = 0.88$). This turned out to be a promising result for further improvement of utilizing high-throughput phenotypic data in sorghum breeding program, as well as accelerating the breeding process.

In the case of analyzing winter wheat final grain yield, three types of feature were calculated from UAV-derived VI and plant height maps: statistical feature (e.g. median), texture feature (e.g. homogeneity calculated from gray-level co-occurrence matrix, GLCM), and growth dynamic feature (growth rate). Including all parameters associated with these types of features, two variable selection methods were adopted to select principal parameters that contribute most to final grain yield. This work could serve as a

reference study for data process and analysis in grain yield estimation, especially in the case when large number of parameters are available but without knowing which variable sets are most critical.

Future work and improvements are needed to allow UAV-based high-throughput phenotyping technique fully utilized and more user friendly. For example, most of the phenotypic traits in current studies were calculated from stitched image that had lower spatial resolution than un-stitched images. It is possible to acquire phenotypic traits with higher accuracy if they were directly calculated using un-stitched images. Utilizing un-stitched images will also decrease the requirement on overlaps between images, thus increasing the potential area covered by one flight. With the recent advances in statistical and machine learning algorithms, it is prospective to mining deeper into UAV aerial imagery to acquire better use of it. In other words, another further work can focus on mining extra information from the aerial imagery, or exploiting the significance of multi-temporal data, using machine-learning technique.

REFERENCE

Andersen, C. M., & Bro, R. (2010). Variable selection in regression-a tutorial. *Journal of Chemometrics*, *24*(11–12), 728–737. https://doi.org/10.1002/cem.1360

Andrade-Sanchez, P., Gore, M. A., Heun, J. T., Thorp, K. R., Carmo-Silva, A. E., French, A., … White, J. W. (2014). Development and evaluation of a field-based , high-thoughput phenotyping platform. *Functional Plant Biology*, *41*(September 2015), 68–79. https://doi.org/10.1071/FP13126

Aparicio, N., Villegas, D., Casadesus, J., Araus, J. L., & Royo, C. (1999). Spectral Vegetation Indices as Nondestructive Tools for Determing Durum Wheat Yield. *Agron.*, *92*(202000), 83–91. https://doi.org/10.2134/agronj2000.92183x

Araus, J. L., & Cairns, J. E. (2014). Field high-throughput phenotyping: The new crop breeding frontier. *Trends in Plant Science*, *19*(1), 52–61. https://doi.org/10.1016/j.tplants.2013.09.008

Araus, J. L., Kefauver, S. C., Zaman-Allah, M., Olsen, M. S., & Cairns, J. E. (2018). Phenotyping: New Crop Breeding Frontier. *Encyclopedia of Sustainability Science and Technology*, 1–11. https://doi.org/10.1007/978-1-4939-2493-6_1036-1

Archer, K. J., & Kimes, R. V. (2008). Empirical characterization of random forest variable importance measures. *Computational Statistics and Data Analysis*, *52*(4), 2249–2260. https://doi.org/10.1016/j.csda.2007.08.015

Asuero, A. G., Sayago, A., & González, A. G. (2006). The correlation coefficient: An overview. *Critical Reviews in Analytical Chemistry*, *36*(1), 41–59. https://doi.org/10.1080/10408340500526766

Bai, G., Ge, Y., Hussain, W., Baenziger, P. S., & Graef, G. (2016). A multi-sensor system for high throughput field phenotyping in soybean and wheat breeding. *Computers and Electronics in Agriculture*, *128*, 181–192. https://doi.org/10.1016/j.compag.2016.08.021

Bandyopadhyay, K. K., Pradhan, S., Sahoo, R. N., Singh, R., Gupta, V. K., Joshi, D. K., & Sutradhar, A. K. (2014). Characterization of water stress and prediction of yield of wheat using spectral indices under varied water and nitrogen management practices. *Agricultural Water Management*, *146*, 115–123. https://doi.org/10.1016/j.agwat.2014.07.017

Belamkar, V., Guttieri, M. J., Hussain, W., Jarquín, D., El-basyoni, I., Poland, J., … Baenziger, P. S. (2018). Genomic Selection in Preliminary Yield Trials in a Winter Wheat Breeding Program. *G3: Genes|Genomes|Genetics*, *8*(8), 2735–2747. https://doi.org/10.1534/g3.118.200415

Bendig, J., Bolten, A., Bennertz, S., Broscheit, J., Eichfuss, S., & Bareth, G. (2014). Estimating biomass of barley using crop surface models (CSMs) derived from UAV-based RGB imaging. *Remote Sensing*, *6*(11), 10395–10412. https://doi.org/10.3390/rs61110395

Bendig, J., Yu, K., Aasen, H., Bolten, A., Bennertz, S., Broscheit, J., … Bareth, G. (2015). Combining UAV-based plant height from crop surface models, visible, and near infrared vegetation indices for biomass monitoring in barley. *International Journal of Applied Earth Observation and Geoinformation*, *39*, 79–87. https://doi.org/10.1016/j.jag.2015.02.012

Benincasa, P., Antognelli, S., Brunetti, L., Fabbri, C. A., Natale, A., Sartoretti, V., … Vizzari, M.

(2018). Reliability of ndvi derived by high resolution satellite and uav compared to in-field methods for the evaluation of early crop n status and grain yield in Wheat. *Experimental Agriculture*, *54*(4), 604–622. https://doi.org/10.1017/S0014479717000278

Bondell, H. D., & Reich, B. J. (2008). Simultaneous regression shrinkage, variable selection, and supervised clustering of predictors with OSCAR. *Biometrics*, *64*(1), 115–123. https://doi.org/10.1111/j.1541-0420.2007.00843.x

Bowman, B. C., Chen, J., Zhang, J., Wheeler, J., Wang, Y., Zhao, W., … Bonman, J. M. (2015). Evaluating grain yield in spring wheat with canopy spectral reflectance. *Crop Science*, *55*(5), 1881–1890. https://doi.org/10.2135/cropsci2014.08.0533

Breiman, L. (2001). Random forests. *Machine Learning*, *45*(1), 5–32. https://doi.org/10.1023/A:1010933404324

Bühlmann, P., Rütimann, P., van de Geer, S., & Zhang, C. H. (2013). Correlated variables in regression: Clustering and sparse estimation. *Journal of Statistical Planning and Inference*, *143*(11), 1835–1858. https://doi.org/10.1016/j.jspi.2013.05.019

Chang, A., Jung, J., Maeda, M. M., & Landivar, J. (2017). Crop height monitoring with digital imagery from Unmanned Aerial System (UAS). *Computers and Electronics in Agriculture*, *141*, 232–237. https://doi.org/10.1016/j.compag.2017.07.008

Chang, A., Jung, J., Yeom, J., Maeda, M., & Landivar, J. (2017). Sorghum panicle extraction from unmanned aerial system data. In *2017 IEEE International Geoscience and Remote Sensing Symposium (IGARSS)* (pp. 4350–4353). IEEE. https://doi.org/10.1109/IGARSS.2017.8127965

Chapman, S., Merz, T., Chan, A., Jackway, P., Hrabar, S., Dreccer, M., … Jimenez-Berni, J. (2014). Pheno-Copter: A Low-Altitude, Autonomous Remote-Sensing Robotic Helicopter for High-Throughput Field-Based Phenotyping. *Agronomy*, *4*(2), 279–301. https://doi.org/10.3390/agronomy4020279

Chu, T., Chen, R., Landivar, J. A., Maeda, M. M., Yang, C., & Starek, M. J. (2016). Cotton growth modeling and assessment using unmanned aircraft system visual-band imagery. *Journal of Applied Remote Sensing*, *10*(3), 036018. https://doi.org/10.1117/1.JRS.10.036018

Comar, A., Burger, P., De Solan, B., Baret, F., Daumard, F., & Hanocq, J. F. (2012). A semi-automatic system for high throughput phenotyping wheat cultivars in-field conditions: Description and first results. *Functional Plant Biology*, *39*(11), 914–924. https://doi.org/10.1071/FP12065

Crain, J., Reynolds, M., & Poland, J. (2017). Utilizing high-throughput phenotypic data for improved phenotypic selection of stress-adaptive traits in wheat. *Crop Science*, *57*(2), 648–659. https://doi.org/10.2135/cropsci2016.02.0135

D. M. Woebbecke, G. E. Meyer, K. Von Bargen, & D. A. Mortensen. (1995). Color Indices for Weed Identification Under Various Soil, Residue, and Lighting Conditions. *Transactions of the ASAE*, *38*(1), 259–269. https://doi.org/10.13031/2013.27838

Das, D. K., Mishra, K. K., & Kalra, N. (1993). Assessing growth and yield of wheat using remotely-sensed canopy temperature and spectral indices. *International Journal of Remote Sensing*, *14*(17), 3081–3092. https://doi.org/10.1080/01431169308904421

de Vlaming, R., & Groenen, P. J. F. (2015). The Current and Future Use of Ridge Regression for Prediction in Quantitative Genetics. *BioMed Research International*, *2015*, 1–18. https://doi.org/10.1155/2015/143712

Degenhardt, F., Seifert, S., & Szymczak, S. (2017). Evaluation of variable selection methods for random forests and omics data sets. *Briefings in Bioinformatics*, (September), 1–12. https://doi.org/10.1093/bib/bbx124

Du, M., & Noguchi, N. (2017). Monitoring of wheat growth status and mapping of wheat yield's within-field spatial variations using color images acquired from UAV-camera System. *Remote Sensing*, *9*(3). https://doi.org/10.3390/rs9030289

Duan, T., Chapman, S. C., Guo, Y., & Zheng, B. (2017a). Dynamic monitoring of NDVI in wheat agronomy and breeding trials using an unmanned aerial vehicle. *Field Crops Research*, *210*(March), 71–80. https://doi.org/10.1016/j.fcr.2017.05.025

Duan, T., Chapman, S. C., Guo, Y., & Zheng, B. (2017b). Dynamic monitoring of NDVI in wheat agronomy and breeding trials using an unmanned aerial vehicle. *Field Crops Research*, *210*(June), 71–80. https://doi.org/10.1016/j.fcr.2017.05.025

Duan, T., Zheng, B., Guo, W., Ninomiya, S., Guo, Y., & Chapman, S. C. (2017). Comparison of ground cover estimates from experiment plots in cotton, sorghum and sugarcane based on images and ortho-mosaics captured by UAV. *Functional Plant Biology*, *44*(1), 169–183. https://doi.org/10.1071/FP16123

Eitel, J. U. H., Long, D. S., Gessler, P. E., & Hunt, E. R. (2008). Combined spectral index to improve ground-based estimates of nitrogen status in dryland wheat. *Agronomy Journal*, *100*(6), 1694–1702. https://doi.org/10.2134/agronj2007.0362

Fernandes, S. B., Dias, K. O. G., Ferreira, D. F., & Brown, P. J. (2018). Efficiency of multi-trait, indirect, and trait-assisted genomic selection for improvement of biomass sorghum. *Theoretical and Applied Genetics*, *131*(3), 747–755. https://doi.org/10.1007/s00122-017-3033-y

Ferrio, J. P., Villegas, D., Zarco, J., Aparicio, N., Araus, J. L., & Royo, C. (2005). Assessment of durum wheat yield using visible and near-infrared reflectance spectra of canopies. *Field Crops Research*, *94*(2–3), 126–148. https://doi.org/10.1016/j.fcr.2004.12.002

Fitzgerald, G. J., Rodriguez, D., Christensen, L. K., Belford, R., Sadras, V. O., & Clarke, T. R. (2006). Spectral and thermal sensing for nitrogen and water status in rainfed and irrigated wheat environments. *Precision Agriculture*, *7*(4), 233–248. https://doi.org/10.1007/s11119-006-9011-z

Fu, Y., Yang, G., Wang, J., & Feng, H. (2013). A comparative analysis of spectral vegetation indices to estimate crop leaf area index. *Intelligent Automation & Soft Computing*, *19*(3), 315–326. https://doi.org/10.1080/10798587.2013.824176

Furbank, R. T., & Tester, M. (2011). Phenomics - technologies to relieve the phenotyping bottleneck. *Trends in Plant Science*, *16*(12), 635–644. https://doi.org/10.1016/j.tplants.2011.09.005

Ge, Y., Bai, G., Stoerger, V., & Schnable, J. C. (2016). Temporal dynamics of maize plant growth, water use, and leaf water content using automated high throughput RGB and

hyperspectral imaging. *Computers and Electronics in Agriculture*, *127*, 625–632. https://doi.org/10.1016/j.compag.2016.07.028

Geipel, J., Link, J., & Claupein, W. (2014). Combined spectral and spatial modeling of corn yield based on aerial images and crop surface models acquired with an unmanned aircraft system. *Remote Sensing*, *6*(11), 10335–10355. https://doi.org/10.3390/rs61110335

Geipel, J., Link, J., Wirwahn, J., & Claupein, W. (2016). A Programmable Aerial Multispectral Camera System for In-Season Crop Biomass and Nitrogen Content Estimation. *Agriculture*, *6*(1), 4. https://doi.org/10.3390/agriculture6010004

Genuer, R., Poggi, J. M., & Tuleau-Malot, C. (2010). Variable selection using random forests. *Pattern Recognition Letters*, *31*(14), 2225–2236. https://doi.org/10.1016/j.patrec.2010.03.014

Girma, K., Martin, K. L., Anderson, R. H., Arnall, D. B., Brixey, K. D., Casillas, M. A., … Raun, W. R. (2006). Mid-season prediction of wheat-grain yield potential using plant, soil, and sensor measurements. *Journal of Plant Nutrition*, *29*(5), 873–897. https://doi.org/10.1080/01904160600649187

Gitelson, A. A., Kaufman, Y. J., & Merzlyak, M. N. (1996). Use of a green channel in remote sensing of global vegetation from EOS-MODIS. *Remote Sensing of Environment*, *58*(3), 289–298. https://doi.org/10.1016/S0034-4257(96)00072-7

Gregorutti, B., Michel, B., & Saint-Pierre, P. (2017). Correlation and variable importance in random forests. *Statistics and Computing*, *27*(3), 659–678. https://doi.org/10.1007/s11222-016-9646-1

Grömping, U. (2009). Variable importance assessment in regression: Linear regression versus random forest. *American Statistician*, *63*(4), 308–319. https://doi.org/10.1198/tast.2009.08199

Guan, S., Fukami, K., Matsunaka, H., Okami, M., Tanaka, R., Nakano, H., … Takahashi, K. (2019). Assessing Correlation of High-Resolution NDVI with Fertilizer Application Level and Yield of Rice and Wheat Crops using Small UAVs. *Remote Sensing*, *11*(2), 112. https://doi.org/10.3390/rs11020112

Guyon, I., & Elisseeff, A. (2011). An Introduction to Variable and Feature Selection. *Journal of Machine Learning Research*, *3*(March), 1157–1182. https://doi.org/10.1016/j.aca.2011.07.027

Haghighattalab, A., Crain, J., Mondal, S., Rutkoski, J., Singh, R. P., & Poland, J. (2017). Application of geographically weighted regression to improve grain yield prediction from unmanned aerial system imagery. *Crop Science*, *57*(5), 2478–2489. https://doi.org/10.2135/cropsci2016.12.1016

Hassan, M. A., Yang, M., Rasheed, A., Jin, X., Xia, X., Xiao, Y., & He, Z. (2018). Time-series multispectral indices from unmanned aerial vehicle imagery reveal senescence rate in bread wheat. *Remote Sensing*, *10*(6). https://doi.org/10.3390/rs10060809

Hassan, M. A., Yang, M., Rasheed, A., Yang, G., Reynolds, M., Xia, X., … He, Z. (2018). A rapid monitoring of NDVI across the wheat growth cycle for grain yield prediction using a multi-spectral UAV platform. *Plant Science*, (October), 1–9.

https://doi.org/10.1016/j.plantsci.2018.10.022

Holman, F. H., Riche, A. B., Michalski, A., Castle, M., Wooster, M. J., & Hawkesford, M. J. (2016). High throughput field phenotyping of wheat plant height and growth rate in field plot trials using UAV based remote sensing. *Remote Sensing*, *8*(12). https://doi.org/10.3390/rs8121031

Hu, P., Chapman, S. C., Wang, X., Potgieter, A., Duan, T., Jordan, D., … Zheng, B. (2018). Estimation of plant height using a high throughput phenotyping platform based on unmanned aerial vehicle and self-calibration: Example for sorghum breeding. *European Journal of Agronomy*, *95*(January), 24–32. https://doi.org/10.1016/j.eja.2018.02.004

Hultquist, C., Chen, G., & Zhao, K. (2014). A comparison of Gaussian process regression, random forests and support vector regression for burn severity assessment in diseased forests. *Remote Sensing Letters*, *5*(8), 723–732. https://doi.org/10.1080/2150704X.2014.963733

Hunt, E. R., & Daughtry, C. S. T. (2018). What good are unmanned aircraft systems for agricultural remote sensing and precision agriculture? *International Journal of Remote Sensing*, *39*(15–16), 5345–5376. https://doi.org/10.1080/01431161.2017.1410300

Hunt, E. R., Dean Hively, W., Fujikawa, S. J., Linden, D. S., Daughtry, C. S. T., & McCarty, G. W. (2010). Acquisition of NIR-green-blue digital photographs from unmanned aircraft for crop monitoring. *Remote Sensing*, *2*(1), 290–305. https://doi.org/10.3390/rs2010290

Iqbal, F., Lucieer, A., Barry, K., & Wells, R. (2017). Poppy crop height and capsule volume estimation from a single UAS flight. *Remote Sensing*, *9*(7), 24–27. https://doi.org/10.3390/rs9070647

Kalubarme, M. H., Potdar, M. B., Manjunath, K. R., Mahey, R. K., & Siddhu, S. S. (2003). Growth profile based crop yield models: A case study of large area wheat yield modelling and its extendibility using atmospheric corrected NOAA AVHRR data. *International Journal of Remote Sensing*, *24*(10), 2037–2054. https://doi.org/10.1080/01431160210156018

Kanning, M., Kühling, I., Trautz, D., Jarmer, T., Kanning, M., Kühling, I., … Jarmer, T. (2018). High-Resolution UAV-Based Hyperspectral Imagery for LAI and Chlorophyll Estimations from Wheat for Yield Prediction. *Remote Sensing 2018, Vol. 10, Page 2000*, *10*(12), 2000. https://doi.org/10.3390/RS10122000

Kefauver, S. C., Vicente, R., Vergara-Díaz, O., Fernandez-Gallego, J. A., Kerfal, S., Lopez, A., … Araus, J. L. (2017a). Comparative UAV and Field Phenotyping to Assess Yield and Nitrogen Use Efficiency in Hybrid and Conventional Barley. *Frontiers in Plant Science*, *8*(October), 1–15. https://doi.org/10.3389/fpls.2017.01733

Kefauver, S. C., Vicente, R., Vergara-Díaz, O., Fernandez-Gallego, J. A., Kerfal, S., Lopez, A., … Araus, J. L. (2017b). Comparative UAV and Field Phenotyping to Assess Yield and Nitrogen Use Efficiency in Hybrid and Conventional Barley. *Frontiers in Plant Science*, *8*(October), 1–15. https://doi.org/10.3389/fpls.2017.01733

Khan, A. J., Azam, F., & Ali, A. (2010). Relationship of morphological traits and grain yield in recombinant inbred wheat lines grown under drought conditions. *Pakistan Journal of Botany*, *42*(1), 259–267.

Kipp, S., Mistele, B., & Schmidhalter, U. (2014). Identification of stay-green and early senescence phenotypes in high-yielding winter wheat, and their relationship to grain yield and grain protein concentration using high-throughput phenotyping techniques. *Functional Plant Biology*, *41*(3), 227–235. https://doi.org/10.1071/FP13221

Kirchgessner, N., Liebisch, F., Yu, K., Pfeifer, J., Friedli, M., Hund, A., & Walter, A. (2017). The ETH field phenotyping platform FIP: A cable-suspended multi-sensor system. *Functional Plant Biology*, *44*(1), 154–168. https://doi.org/10.1071/FP16165

Kyratzis, A. C., Skarlatos, D. P., Menexes, G. C., Vamvakousis, V. F., & Katsiotis, A. (2017). Assessment of Vegetation Indices Derived by UAV Imagery for Durum Wheat Phenotyping under a Water Limited and Heat Stressed Mediterranean Environment. *Frontiers in Plant Science*, *8*(June), 1–14. https://doi.org/10.3389/fpls.2017.01114

Law, C. N., Snape, J. W., & Worland, A. J. (1978). The Genetical Relationship Between Height and Yield in Wheat. *Heredity*, *40*, 133–151.

Lee, K.-J., & Lee, B.-W. (2011). Estimating canopy cover from color digital camera image of rice field. *Journal of Crop Science and Biotechnology*, *14*(2), 151–155. https://doi.org/10.1007/s12892-011-0029-z

Leng, C., Lin, Y., & Wahba, G. (2006). A Note on the Lasso and Related Procedures. *Statistica Sinica*, *16*, 1273–1284.

Li, J., Shi, Y., Veeranampalayam-Sivakumar, A.-N., & Schachtman, D. P. (2018). Elucidating Sorghum Biomass, Nitrogen and Chlorophyll Contents With Spectral and Morphological Traits Derived From Unmanned Aircraft System. *Frontiers in Plant Science*, *9*(October), 1–12. https://doi.org/10.3389/fpls.2018.01406

Li, L., Mu, X., Macfarlane, C., Song, W., Chen, J., Yan, K., & Yan, G. (2018). A half-Gaussian fitting method for estimating fractional vegetation cover of corn crops using unmanned aerial vehicle images. *Agricultural and Forest Meteorology*, *262*(July), 379–390. https://doi.org/10.1016/j.agrformet.2018.07.028

Lichtenthaler, H. K., & Wellburn, A. R. (1983). Determinations of total carotenoids and chlorophylls a and b of leaf extracts in different solvents. *Biochemical Society Transactions*, *11*, 591–592.

Liu, Y., Mu, X., Wang, H., & Yan, G. (2012). A novel method for extracting green fractional vegetation cover from digital images. *Journal of Vegetation Science*, *23*(3), 406–418. https://doi.org/10.1111/j.1654-1103.2011.01373.x

Lu, F., & Petkova, E. (2014). A comparative study of variable selection methods in the context of developing psychiatric screening instruments. *Stat Med.*, *33*(3), 401–421. https://doi.org/10.1002/sim.5937.A

Makino, A. (2010). Photosynthesis, Grain Yield, and Nitrogen Utilization in Rice and Wheat. *Plant Physiology*, *155*(1), 125–129. https://doi.org/10.1104/pp.110.165076

Malambo, L., Popescu, S. C., Murray, S. C., Putman, E., Pugh, N. A., Horne, D. W., … Bishop, M. (2018). Multitemporal field-based plant height estimation using 3D point clouds generated from small unmanned aerial systems high-resolution imagery. *International Journal of Applied Earth Observation and Geoinformation*, *64*(June 2017), 31–42.

https://doi.org/10.1016/j.jag.2017.08.014

McDonald, G. C. (2009). Ridge regression. *Wiley Interdisciplinary Reviews: Computational Statistics*, *1*(1), 93–100. https://doi.org/10.1002/wics.14

Mohanaiah, P., Sathyanarayana, P., & Gurukumar, L. (2013). Image Texture Feature Extraction Using GLCM Approach. *International Journal of Scientific and Research Publications*, *3*(1), 2250–3153. https://doi.org/10.1.1.414.96981

Montesinos-López, O. A., Montesinos-López, A., Crossa, J., los Campos, G., Alvarado, G., Suchismita, M., … Burgueño, J. (2017). Predicting grain yield using canopy hyperspectral reflectance in wheat breeding data. *Plant Methods*, *13*(1), 1–23. https://doi.org/10.1186/s13007-016-0154-2

Moravec, D., Komárek, J., Kumhálová, J., Kroulík, M., Prošek, J., & Klápště, P. (2017). Digital elevation models as predictors of yield: Comparison of an UAV and other elevation data sources. *Agronomy Research*, *15*(1), 249–255.

Mutanga, O., & Skidmore, A. K. (2004). Narrow band vegetation indices overcome the saturation problem in biomass estimation. *International Journal of Remote Sensing*, *25*(19), 3999–4014. https://doi.org/10.1080/01431160310001654923

Orhan, H., Eyduran, E., Tatliyer, A., & Saygici, H. (2016). Prediction of egg weight from egg quality characteristics via ridge regression and regression tree methods. *Revista Brasileira de Zootecnia*, *45*(7), 380–385. https://doi.org/10.1590/S1806-92902016000700004

Potgieter, A. B., George-Jaeggli, B., Chapman, S. C., Laws, K., Suárez Cadavid, L. A., Wixted, J., … Hammer, G. L. (2017). Multi-Spectral Imaging from an Unmanned Aerial Vehicle Enables the Assessment of Seasonal Leaf Area Dynamics of Sorghum Breeding Lines. *Frontiers in Plant Science*, *8*(September), 1–11. https://doi.org/10.3389/fpls.2017.01532

Prasad, B., Carver, B. F., Stone, M. L., Babar, M. A., Raun, W. R., & Klatt, A. R. (2007). Genetic analysis of indirect selection for winter wheat grain yield using spectral reflectance indices. *Crop Science*, *47*(4), 1416–1425. https://doi.org/10.2135/cropsci2006.08.0546

Ramatoulaye, F., Mady, C., Fallou, S., Amadou, K., Cyril, D., Massamba, D., & Diouf, M. (2016). Production and Use Sorghum: A Literature Review. *Journal of Nutritional Health & Food Science*, 2–5. https://doi.org/10.15226/jnhfs.2016.00157

Ray, D. K., Mueller, N. D., West, P. C., & Foley, J. A. (2013). Yield Trends Are Insufficient to Double Global Crop Production by 2050. *PLoS ONE*, *8*(6). https://doi.org/10.1371/journal.pone.0066428

Rischbeck, P., Elsayed, S., Mistele, B., Barmeier, G., Heil, K., & Schmidhalter, U. (2016). Data fusion of spectral, thermal and canopy height parameters for improved yield prediction of drought stressed spring barley. *European Journal of Agronomy*, *78*, 44–59. https://doi.org/10.1016/j.eja.2016.04.013

Roujean, J. L., & Breon, F. M. (1995). Estimating PAR absorbed by vegetation from bidirectional reflectance measurements. *Remote Sensing of Environment*, *51*(3), 375–384. https://doi.org/10.1016/0034-4257(94)00114-3

Sankaran, S., Khot, L. R., Espinoza, C. Z., Jarolmasjed, S., Sathuvalli, V. R., Vandemark, G. J.,

… Pavek, M. J. (2015). Low-altitude, high-resolution aerial imaging systems for row and field crop phenotyping: A review. *European Journal of Agronomy*, *70*, 112–123. https://doi.org/10.1016/j.eja.2015.07.004

Schirrmann, M., Giebel, A., Gleiniger, F., Pflanz, M., Lentschke, J., & Dammer, K. H. (2016). Monitoring agronomic parameters of winter wheat crops with low-cost UAV imagery. *Remote Sensing*, *8*(9). https://doi.org/10.3390/rs8090706

Schlemmera, M., Gitelson, A., Schepersa, J., Fergusona, R., Peng, Y., Shanahana, J., & Rundquist, D. (2013). Remote estimation of nitrogen and chlorophyll contents in maize at leaf and canopy levels. *International Journal of Applied Earth Observation and Geoinformation*, *25*(1), 47–54. https://doi.org/10.1016/j.jag.2013.04.003

Serrano, L., Filella, I., & Penuelas, J. (2000). Remote sensing of biomass and yield of winter wheat under different nitrogen supplies. *Crop Science*, *40*, 723–731. https://doi.org/10.2135/cropsci2000.403723x

Shafian, S., Rajan, N., Schnell, R., Bagavathiannan, M., Valasek, J., Shi, Y., & Olsenholler, J. (2018). Unmanned aerial systems-based remote sensing for monitoring sorghum growth and development.

Shi, Y., Thomasson, J. A., Murray, S. C., Pugh, N. A., Rooney, W. L., Shafian, S., … Yang, C. (2016). Unmanned Aerial Vehicles for High-Throughput Phenotyping and Agronomic Research. *PloS One*, *11*(7), e0159781. https://doi.org/10.1371/journal.pone.0159781

Snavely, N., Seitz, S. M., & Szeliski, R. (2008). Modeling the World from Internet Photo Collections. *International Journal of Computer Vision*, *80*(2), 189–210. https://doi.org/10.1007/s11263-007-0107-3

Stanton, C., Starek, M. J., Elliott, N., Brewer, M., Maeda, M. M., & Chu, T. (2017). Unmanned aircraft system-derived crop height and normalized difference vegetation index metrics for sorghum yield and aphid stress assessment. *Journal of Applied Remote Sensing*, *11*(2), 026035. https://doi.org/10.1117/1.JRS.11.026035

Sun, W., Zhang, L., Du, B., Li, W., & Mark Lai, Y. (2015). Band Selection Using Improved Sparse Subspace Clustering for Hyperspectral Imagery Classification. *IEEE Journal of Selected Topics in Applied Earth Observations and Remote Sensing*, *8*(6), 2784–2797. https://doi.org/10.1109/JSTARS.2015.2417156

Svensgaard, J., Roitsch, T., & Christensen, S. (2014). Development of a Mobile Multispectral Imaging Platform for Precise Field Phenotyping. *Agronomy*, *4*(3), 322–336. https://doi.org/10.3390/agronomy4030322

Texas, J. J., Christi, C., Texas, S. C. P. S., Texas, S. C. P. S., Christi, C., Texas, B., … Rooney, W. L. (2018). Temporal Estimates of Crop Growth in Sorghum and Maize Breeding Enabled by Unmanned Aerial Systems. *The Plant Phenome Journal*, *1*, 1–10. https://doi.org/10.2135/tppj2017.08.0006

Tibshirani, R. (1996). Regression Shrinkage and Selection via the Lasso Author (s): Robert Tibshirani Source : Journal of the Royal Statistical Society . Series B (Methodological), Vol . 58 , No . 1 Published by : Blackwell Publishing for the Royal Statistical Society Stabl, *58*(1), 267–288.

Tilly, N., Aasen, H., & Bareth, G. (2015). Fusion of plant height and vegetation indices for the estimation of barley biomass. *Remote Sensing*, *7*(9), 11449–11480. https://doi.org/10.3390/rs70911449

Vapnik, V., Golowich, S. E., & Alex, S. (1997). Support Vector Method for Function Approximation, Regression Estimation, and Signal Processing, 281–287. https://doi.org/10.1007/978-3-662-45789-4_5

Varela, S., Assefa, Y., Vara Prasad, P. V., Peralta, N. R., Griffin, T. W., Sharda, A., … Ciampitti, I. A. (2017). Spatio-temporal evaluation of plant height in corn via unmanned aerial systems. *Journal of Applied Remote Sensing*, *11*(03), 1. https://doi.org/10.1117/1.JRS.11.036013

Virlet, N., Sabermanesh, K., Sadeghi-Tehran, P., & Hawkesford, M. J. (2017). Field Scanalyzer: An automated robotic field phenotyping platform for detailed crop monitoring. *Functional Plant Biology*, *44*(1), 143–153. https://doi.org/10.1071/FP16163

Vos, R., & Bellù, L. G. (2019). Global Trends and Challenges to Food and Agriculture into the 21st Century. *Sustainable Food and Agriculture*, 11–30. https://doi.org/10.1016/b978-0-12-812134-4.00002-9

Wang, L., Tian, Y., Yao, X., Zhu, Y., & Cao, W. (2014). Predicting grain yield and protein content in wheat by fusing multi-sensor and multi-temporal remote-sensing images. *Field Crops Research*, *164*(1), 178–188. https://doi.org/10.1016/j.fcr.2014.05.001

Wang, L., Zhou, X., Zhu, X., Dong, Z., & Guo, W. (2016). Estimation of biomass in wheat using random forest regression algorithm and remote sensing data. *Crop Journal*, *4*(3), 212–219. https://doi.org/10.1016/j.cj.2016.01.008

Watanabe, K., Guo, W., Arai, K., Takanashi, H., Kajiya-Kanegae, H., Kobayashi, M., … Iwata, H. (2017). High-Throughput Phenotyping of Sorghum Plant Height Using an Unmanned Aerial Vehicle and Its Application to Genomic Prediction Modeling. *Frontiers in Plant Science*, *8*(March), 1–11. https://doi.org/10.3389/fpls.2017.00421

White, J. W., Andrade-Sanchez, P., Gore, M. A., Bronson, K. F., Coffelt, T. A., Conley, M. M., … Wang, G. (2012). Field-based phenomics for plant genetics research. *Field Crops Research*, *133*, 101–112. https://doi.org/10.1016/j.fcr.2012.04.003

Yang, G., Liu, J., Zhao, C., Li, Z., Huang, Y., Yu, H., … Yang, H. (2017). Unmanned Aerial Vehicle Remote Sensing for Field-Based Crop Phenotyping: Current Status and Perspectives. *Frontiers in Plant Science*, *8*(June). https://doi.org/10.3389/fpls.2017.01111

Yendrek, C. R., Tomaz, T., Montes, C. M., Cao, Y., Morse, A. M., Brown, P. J., … Ainsworth, E. A. (2017). High-Throughput Phenotyping of Maize Leaf Physiological and Biochemical Traits Using Hyperspectral Reflectance. *Plant Physiology*, *173*(1), 614–626. https://doi.org/10.1104/pp.16.01447

Yue, J., Yang, G., Li, C., Li, Z., Wang, Y., Feng, H., & Xu, B. (2017). Estimation of winter wheat above-ground biomass using unmanned aerial vehicle-based snapshot hyperspectral sensor and crop height improved models. *Remote Sensing*, *9*(7). https://doi.org/10.3390/rs9070708

Zhang, C. H., & Huang, J. (2008). The sparsity and bias of the lasso selection in high-dimensional linear regression. *Annals of Statistics*, *36*(4), 1567–1594.

https://doi.org/10.1214/07-AOS520

Zhang, M., Wei, S., Sun, H., Qiu, R., Li, M., Liu, G., & Li, H. (2018). Sensors for measuring plant phenotyping: A review. *International Journal of Agricultural and Biological Engineering*, *11*(2), 1–17. https://doi.org/10.25165/j.ijabe.20181102.2696

Zhang, Z., Masjedi, A., Zhao, J., & Crawford, M. M. (2017). Prediction of sorghum biomass based on image based features derived from time series of UAV images. *International Geoscience and Remote Sensing Symposium (IGARSS)*, *2017–July*, 6154–6157. https://doi.org/10.1109/IGARSS.2017.8128413